J. Fluid Mech. (1986), *vol.* 173, *pp.* 303–356
Printed in Great Britain

Coherent structures and turbulence

By A. K. M. FAZLE HUSSAIN
University of Houston, TX 77004, USA

(Received 9 May 1986)

This is a personal statement on the present state of understanding of coherent structures, in particular their spatial details and dynamical significance. The characteristic measures of coherent structures are discussed, emphasizing coherent vorticity as the crucial property. We present here a general scheme for educing structures in any transitional or fully turbulent flow. From smoothed vorticity maps in convenient flow planes, this scheme recognizes patterns of the same mode and parameter size, and then phase-aligns and ensemble-averages them to obtain coherent structure measures. The departure of individual realizations from the ensemble average denotes incoherent turbulence. This robust scheme has been used to educe structures from velocity data using a rake of hot wires as well as direct numerical simulations and can educe structures using newer measurement techniques such as digital image processing. Our recent studies of coherent structures in several free shear flows are briefly reviewed. Detailed data in circular and elliptic jets, mixing layers, and a plane wake reveal that incoherent turbulence is produced at the 'saddles' and then advected to the 'centres' of the structures. The mechanism of production of turbulence in shear layers is the stretching of longitudinal vortices or 'ribs' which connect the predominantly spanwise 'rolls'; the ribs induce spanwise contortions of rolls and cause mixing and dissipation, mostly at points where they connect with rolls. We also briefly discuss the role of coherent structures in aerodynamic noise generation and argue that the structure breakdown process, rather than vortex pairing, is the dominant mechanism of noise generation. The 'cut-and-connect' interaction of coherent structures is proposed as a specific mechanism of aerodynamic noise generation, and a simple analytical model of it shows that it can provide acceptable predictions of jet noise. The coherent-structures approach to turbulence, apart from explaining flow physics, has also enabled turbulence management via control of structure evolution and interactions. We also discuss some new ideas under investigation: in particular, helicity as a characteristic property of coherent structures.

CONTENTS

1. Introduction

1.1. *Revolution one – coherent structures*

So profound has been the impact of coherent structures that virtually every turbulence researcher is pursuing them in one form or another. Coherent structures are the embodiment of our desire to find order in apparent disorder. The popularity of coherent structures should be evident from the fact that the literature in this field runs into thousands of papers, and a healthy number of review papers (for example: Kline *et al.* 1967; Crow & Champagne 1971; Roshko 1976; Kovasznay 1977; Smith & Abbott 1978; Saffman 1980; Cantwell 1981; Lumley 1981; Coles 1981, 1985; Antonia 1981; Keffer 1982; Laufer 1983; Ho & Huerre 1984; Rogallo & Moin 1984) have been published.

Large-scale organized transports were implicit in the mixing length and vorticity transport theories of Prandtl and Taylor as well as in the works of Wille, Townsend, Grant and others. Explicit recognition of the presence and role of organized structures was apparent in the works of Brown (1935), Anderson (1954), Bradshaw, Ferriss & Johnson (1964), Mollo-Christensen (1967) and others. However, the widespread occurrence and dominant role of coherent structures in turbulence phenomena have become clear only recently through the works of Kline, Hama, Klebanoff, Roshko, Crow, Coles, Browand, Kovasznay, Laufer, Kaplan, Brodkey, Willmarth and others. Coherent structures were evident in prior flow-visualization studies, especially in the transitional regions of shear flows, but escaped attention and emphasis because of the preoccupation with fully developed turbulent regions, where similarity scaling was expected to hold. Claims that coherent structures have brought about a redefinition of turbulence are clearly overstatements, even though some of the established notions

of turbulence are at variance with the findings of coherent-structures research and need to be modified or rationalized. Coherent structures have not only raised many more questions than they have answered, but also have injected new momentum and excitement into turbulence research.

1.2. *Revolution two – digital computer as a turbulence research tool*

A second revolution in turbulence research in recent years has been the incorporation of the digital computer as an integral (even interactive) component of the turbulence research arsenal. The computer is now commonly used not only as a versatile laboratory instrument (to measure various turbulence quantities) but also for experiment control and acquisition (including conditional sampling) and analysis (including pattern recognition) of data. Moreover, with the advent of supercomputers, direct numerical simulations of turbulent flows via time-evolving solutions of the complete Navier–Stokes equations in three-dimensional space are now possible, at least at moderate Reynolds numbers (e.g. Moin & Kim 1985).

Both computer experiments (i.e. simulations) and laboratory experiments have their limitations. Simulation allows systematic variations as well as precise control of initial and boundary conditions and thus allows studies of their effects on the flow field. This is not always possible in laboratory experiments. Via numerical simulation one can 'measure' quantities such as vorticity, enstrophy, dissipation, pressure, etc. which are impossible to measure accurately in the laboratory. Simultaneous measurement of the flow-field evolution, like those computed numerically, will be prohibitively expensive and will be subject to unacceptable errors due to probe interference. Avoidance of such interference forces the use of Taylor's hypothesis, the validity of which to turbulent shear flows is in doubt (Lin 1953; Fisher & Davies 1964; Lumley 1965; Heskestad 1965; Champagne 1978).

Two outstanding constraints of numerical simulation are the Reynolds number of the flow and the number of repeats or the duration of flow that can be computed. The first is a technological limit, the second is economic. The Reynolds number of flows that can be computed directly is rather small in comparison with practical or even laboratory flows. Thus fine scales of practical turbulent flows cannot be resolved. Also, the flow time that can be economically computed is far too short. For eduction of coherent structures, the number of realizations required is large. Also, in situations such as phase space analysis of flow variables, extremely long time records are required. Adequate computation time for either purpose will be prohibitively expensive.

Clearly, computer and laboratory experiments play complementary roles (e.g. Metcalfe *et al.* 1986*a*), and computer experiments cannot yet resolve details of flows at practical Reynolds numbers and thus cannot replace laboratory experiments. Laboratory experimentation will continue to be important not only for understanding the physics of unsteady, vortex, or turbulent flows, but also for 'calibration' of numerical codes.

2. The nature of coherent structures

2.1. *Earlier approaches – flow visualization*

Virtually all coherent structure studies have been based on flow visualization only. But it has its limitations. The flow marker (such as dye or smoke) is typically introduced at the point of flow initiation. Sufficiently far downstream, in a turbulent flow, the marker outline has little to do with the boundary of the turbulent domain.

First, the markers are smeared rapidly so that the local flow dynamics cannot be clearly discerned. The markers reflect the integration of the history of the motions they have undergone since their injection in the flow. Also, because of the rapid (i.e. turbulent) diffusion of the markers, their concentration as well as the sharpness of their fronts decreases with increasing evolution time or distance from the point of injection. Clearer perception of the local flow dynamics can be obtained if the markers can be introduced locally. That is why hydrogen-bubble or smoke wires are often preferable.

Even in a laminar flow, marker boundaries can be largely different from vortex boundaries. One example is that of the laminar wake of a cylinder at low Reynolds numbers ($Re_d \approx 140$). Many investigators have been misled by the long survival of smoke or dye markers introduced at the cylinder, and they have surmised indefinite survival of shed laminar vortices. The molecular diffusivities of vorticity and markers being very different (i.e. the Schmidt number being large), vorticity should be expected to have diffused away from the smoke-marked fluid. Also, Taneda (1959) has shown that the initial vortices undergo breakdown and decay by about $x/d = 80$ before a new vortex structure is formed, perhaps as an instability of the local flow (presumably *not* of the mean wake profile). The misinterpretation of smoke lumps in cylinder wakes and wake instability have been re-examined recently by Cimbala (1984). Another example of the contrast between marker pictures and the organized structures is evident from jet flow pictures of Dimotakis, Lye & Papantoniou (1982). Even though pictures showing markers splintered into innumerable tiny domains suggest that there are no large-scale coherent structures in the far field, structures scaling on the far-field jet diameter do occur; these structures have been educed and their dynamics studied in some detail by Tso (discussed in §3.5.2).

Clearly, flow visualization is extremely useful and should be tried whenever possible, but only as a supplement to quantitative measurements. Digital image processing is a welcome blending of both visualization and simultaneous measurement over a flow domain, and is emerging as a powerful research tool. Also, most visualizations of coherent structures have been carried out at low Reynolds numbers – typically motivated by the ease of interpretation (for example, Reynolds & Bouchard 1981; Perry & Chong 1982; Perry & Tan 1984). However, one must not assume the same phenomena to occur at higher Reynolds numbers as the flow physics can be, and often are, highly Reynolds-number-dependent, except perhaps in the very high Reynolds-number range.

What is needed is a description of a coherent structure in three-dimensional space, as the structures are in general three-dimensional. While this can be done easily for structures educed from direct numerical simulations, it will be virtually impossible to do so experimentally because of constraints of measurement technology – constraints due to the limited number of sensors forced by cost, space and computer (memory size, and digitization and data transfer rates). Laboratory measurements will thus miss the flow physics, which can be captured only in a three-dimensional eduction.

2.2. *Definition and characteristics of coherent structures*

There is as yet no consensus in what is meant by coherent structures. Most researchers have seen pictures of structures in a mixing layer, first emphasized by Brown & Roshko (1974). Granted, there is some superficial consensus on qualitative aspects of the Brown–Roshko structure, but there is very little regarding structures in other flows. Even in the plane mixing layer, the structure is far more complicated and three-dimensional (Metcalfe *et al.* 1986*a*) than indicated by the Brown–Roshko and subsequent studies (e.g. Browand & Troutt 1985).

In principle, concepts like coherent structures are best left implicit; efforts to provide a precise definition may seem pedantic. However, the need to measure coherent structures and assess their dynamical significance motivated me to construct a definition of coherent structures. *A coherent structure is a connected turbulent fluid mass with instantaneously phase-correlated vorticity over its spatial extent* (see Hussain 1980, 1981, 1983*a*). That is, underlying the random, three-dimensional vorticity that characterizes turbulence, there is a component of large-scale vorticity which is instantaneously coherent over the spatial extent of a coherent structure. We choose to designate the instantaneously space- and phase-correlated vorticity as *coherent vorticity*. Thus, coherent vorticity is the primary identifier of coherent structures, which have distinct boundaries and independent territories. The identification with fluid mass in the definition is not intended to mean that structure evolution is by advection alone, as structure size (and also shape) changes by entrainment, pairing, tearing and crosslinking.

As a consequence of this definition, a turbulent shear flow can be decomposed into coherent structures and incoherent turbulence. Implicit in the definition is the operation of ensemble averaging to identify a coherent structure. The ensemble average of appropriately phase-aligned realizations containing similar organized events is a coherent structure; whatever is not included in the ensemble average is incoherent turbulence. As should be clear later on, this separation of the total field is conceptually precise, but operationally non-unique: incoherent turbulence does not consist of only fine-scale turbulence, as is generally presumed, but may contain large-scale irrotational (perhaps even vortical but irrelevant) motions. The interaction between coherent structures and incoherent turbulence is the most critical and least understood aspect of turbulent shear flows. This coupling appears to be rather different from the classical notion of cascade; even considering the large and fine scales, they are not decoupled as widely presumed. The coupling can be intricate and of different kinds; see §4.3 for an example.

The purpose of eduction is to separate from instantaneous flow fields the coherent and incoherent parts. We use *phase average* to denote phase-aligned ensemble average. This is an average of successive structures at the same phase or age, but not an average over all phases; the latter would be meaningless. Thus, the phase average of structures of the same mode and parameter size is the coherent structure, and the departure of each instantaneous realization from the phase average denotes incoherent turbulence.

In turbulent *free* shear flows, which have been the focus of most studies of coherent structures so far, by coherent structures we mean those which are large-scale, even when this adjective is not included. This is because they are dynamically more significant than other structures. Turbulence at the Kolmogorov scale η is obviously the most coherent as significant vorticity (and of course, velocity or pressure) variations cannot occur over this scale; turbulence at this scale is not dynamically dominant. By coherent structures, we mean those of size comparable to the transverse lengthscale l of the shear flow. Thus the Reynolds number vl/ν is large (as compared to $v\eta/\nu \approx 1$ for the Kolmogorov scale where v is a measure of the turbulence velocity), and hence the coherent structure dynamics are inviscid, the viscous effect being extremely remote (only via the smallest scales around η). Intermediate-scale coherent motions such as 'ribs', 'hairpins', 'typical eddies' also occur. (Their cross-sectional size is usually of the order of the Taylor microscale λ.) To be consistent, we will call them *coherent substructures*. For example, in wall-bounded flows, these substructures can be dynamically significant and are worthy of eduction (say, via the eduction scheme discussed in §3.4) and detailed investigation.

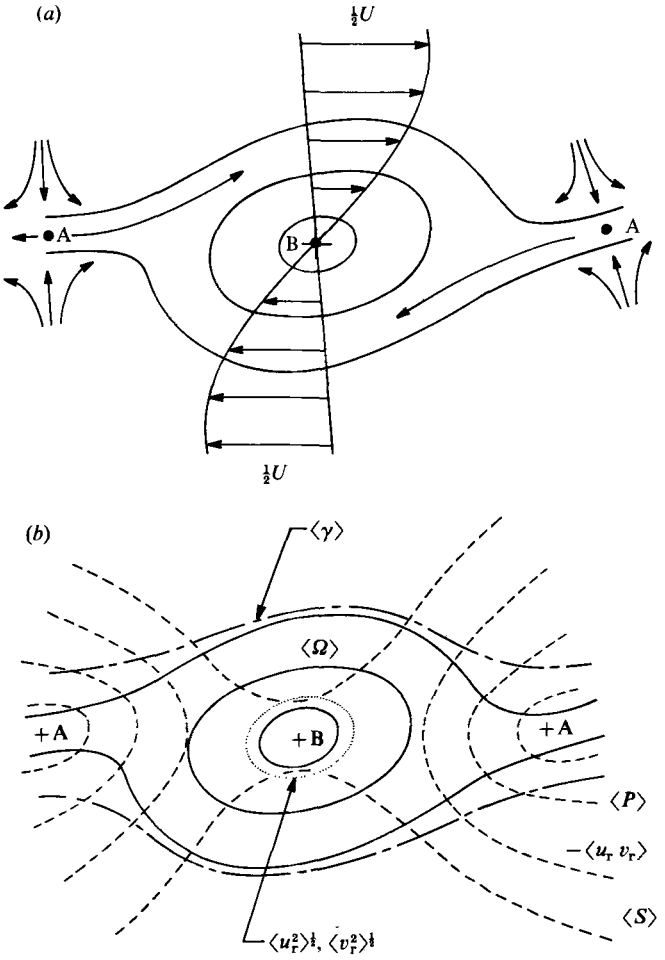

FIGURE 1. An example of a coherent structure in a plane mixing layer. (*a*) Coherent vorticity $\langle\Omega\rangle$ contours and saddle A and centre B; (*b*) approximate contours of other coherent structure properties: coherent intermittency $\langle\gamma\rangle$; incoherent turbulence intensities $\langle u_r^2\rangle^{\frac{1}{2}}$, $\langle v_r^2\rangle^{\frac{1}{2}}$; incoherent Reynolds stress $-\langle u_r v_r\rangle$; coherent strain rate $\langle S\rangle$; coherent production $\langle P\rangle$.

Figure 1(*a*) shows an example of the spanwise cut of a coherent structure, in particular in the plane mixing layer. The outer contour of coherent vorticity $\langle\Omega\rangle$ denotes the structure boundary; this boundary, but not the structure strength, will, of course, depend on the coherent vorticity threshold used. Note that there are two critical points: the saddle (A) characterized by negligible spanwise coherent vorticity, and the centre (B) characterized by peak spanwise coherent vorticity. Also shown qualitatively are contours of coherent strain rate $\langle S\rangle$; incoherent turbulence intensities $\langle u_r^2\rangle^{\frac{1}{2}}$, $\langle v_r^2\rangle^{\frac{1}{2}}$; incoherent Reynolds stress $-\langle u_r v_r\rangle$; coherent intermittency $\langle\gamma\rangle$; and coherent production $\langle P\rangle$ (figure 1*b*). Contours of $\langle S\rangle$, $-\langle u_r v_r\rangle$, and $\langle P\rangle$ are similar; thus their differences are not emphasized here.

2.3. *Quantitative approaches*

For quantitative aspects of coherent structures, there must be a clear delineation of an operational procedure for their measurement. Two separate ways of analysing coherent structures have been followed: *triple* and *double decompositions*, mentioned

briefly in Appendix A and discussed by Hussain (1983*a*). Turbulent flows consist of both coherent and incoherent motions at various scales. To encompass the whole range of motions realistically, the flow field should perhaps be decomposed into a mean, and a hierarchy of both coherent and incoherent motions of various scales. Accounting for all these motions separately will be cumbersome experimentally. Analytically, such decomposition will merely compound the closure problem. Thus we chose the simpler decompositions, which enable us to focus on dynamically significant events. Clearly, 'mean' flow will take on different meanings under different decompositions. This is why arguments based on 'mean flow' or 'mean shear' should be viewed as tentative; they are also mostly devoid of instantaneous flow physics.

The process of measuring the properties of a structure over its spatial extent is now popularly known as *eduction*. The eduction process is based on a number of conceptual arguments and operational procedures; we will first discuss the general concepts, and then explain our eduction scheme and its application to a few flows.

2.3.1. *Preferred mode*

Eduction implies ensemble averaging a large number of 'similar' structures or organized events and is meaningful only for a 'preferred' mode. By mode we mean the physical configuration (e.g. roller, toroidal, helical, bihelical, hairpin, etc.). In general, vortical structures have a large dispersion in the characteristic parameters such as shape, size, strength, orientation, convection velocity, etc. A point in this parameter space, i.e. a set of particular values of the structure parameters, denotes a parameter size. Now if in the parameter space the (multi-dimensional) probability density function has a few isolated peaks, these are called preferred modes. Of all possible structures in a turbulent shear flow, it may suffice to study these modes alone, as they should dominate the flow physics. Typically, only a few peaks are expected to occur. If one peak is much higher than the others we call it the dominant preferred mode, or simply the preferred mode – the mode which deserves detailed investigation first.

Implicit in the concept of coherent structures is the concept of preferred mode(s). In fact, the coherent-structures approach to turbulence is helpful only if preferred modes occur. Some researchers believe that a turbulent shear flow can have numerous or even an infinite variety of coherent structures. If that is true the coherent structures concept is useless. Eduction of a variety of coherent structures will be virtually impossible not only on account of the total effort involved, but also because a long time will be required to capture a sufficient number of similar structures to obtain a true ensemble average for each subclass of structures. One must also state the probability of occurrence and relative significance of each structure. Furthermore, even if all details of all coherent structures were known, one would need to have recourse to an elaborate statistical approach in order to incorporate them all into a theory. It is not obvious that such a theory will be simple or even useful.

Thus the key problem in eduction is classifying structures into different subclasses, capturing structures of one subclass at a time, phase-aligning them and then obtaining ensemble averages. This is a painstaking task to which no simplification seems to be available. One can easily be tempted to capture a single realization and then spatially smooth it. We philosophically disagree with this approach, as coherent structures are defined as statistical entities, and as there is no way to know *a priori* how much of the flow variables are coherent and how much incoherent; also, one has no way of knowing if the captured event is typical or 'freak'. There are objections to the procedure too. Such smoothing would be meaningful only if the organized

motions are of one mode and size (i.e. all structures are identical) and if the incoherent turbulence is truly fine-scale; as we have discussed, this is not necessarily so. Even if this were true, spatial smoothing to obtain a coherent structure from a single realization does not seem to be reasonable because: there is no test for convergence of smoothing via a spatial filter; since the filter spatial size must vary over the structure, there is no way of determining the spatial variation of the filter size; and such spatial filtering removes sharp fronts or gradients which will be retained in properly phase-aligned ensemble averaging.

2.4. *Further implications of coherent structure definition*

Quantitative studies of coherent structures are very few. Of these, most involve correlation of velocity, pressure or intermittency to identify coherent structures. We have explained why these correlations cannot unambiguously identify coherent structures (Hussain 1983*a*). The intermittency signal that detects turbulent/non-turbulent interface can be used to detect coherent structures only qualitatively (and only in flows which are bounded by irrotational ambient flows) provided that incoherent turbulence can be assumed to be totally embedded within coherent structures. Such is not true in general; see the difference between contours of coherent vorticity and intermittency in figure 1(*b*). An intermittency signal will be clearly useless for educing coherent structures in turbulent pipe or channel flows, in the wall region of turbulent boundary layers, or even in fully developed jets and wakes. Another limitation of pressure or velocity correlation is that it extends far beyond the structure boundary (defined by coherent vorticity). Michalke (private communication, 1983) raises an interesting point of view by claiming that vorticity is the 'skeleton' of a coherent structure and the induced flow field denotes its 'body'. We insist on delimiting the boundary on the basis of coherent vorticity.

Coherent structures play important roles in transports of heat, mass and momentum (hence combustion, chemical reaction and drag) as well as aerodynamic noise generation, but they themselves are not necessarily highly energetic. This statement needs clarification. In transitional flows, coherent structures are indeed energetic and are dominant in turbulence phenomena. In fully turbulent flows, they share these roles with incoherent turbulence, the contributions of both to turbulence phenomena being comparable.

Coherent structures are spatially non-overlapping; each has its own territory. Thus cascade is not a relevant concept for coherent structure interactions. Cascade may still be a useful concept for energy exchange between different scales within incoherent turbulence or even between coherent structures and incoherent turbulence. The interactions of coherent structures are intrinsically nonlinear, typically involving pairing or tearing. Pairing, which suggests amalgamation of two structures (figure 2*a*) has been discussed at length by Winant & Browand (1974) and Hussain & Zaman (1980). In addition to complete pairing just mentioned, there can be fractional pairing (figure 2*b*) or partial pairing (figure 2*c*), discussed by Hussain & Clark (1981). Tearing (figure 2*d*) occurs when a structure is torn into two or more parts (see Moore & Saffman 1975). Unlike cascade, when 'eddies' of different scales superimposed on the same space are presumed to exist in equilibrium (Tennekes & Lumley 1974), interactions of coherent structures always produce newer structures of different scales.

The definition of coherent structures in terms of coherent vorticity has been the focus of some controversy, but now appears to have gradually gained wide acceptance. However, even today, most other studies of coherent structures neither address coherent vorticity nor use it to educe coherent structures.

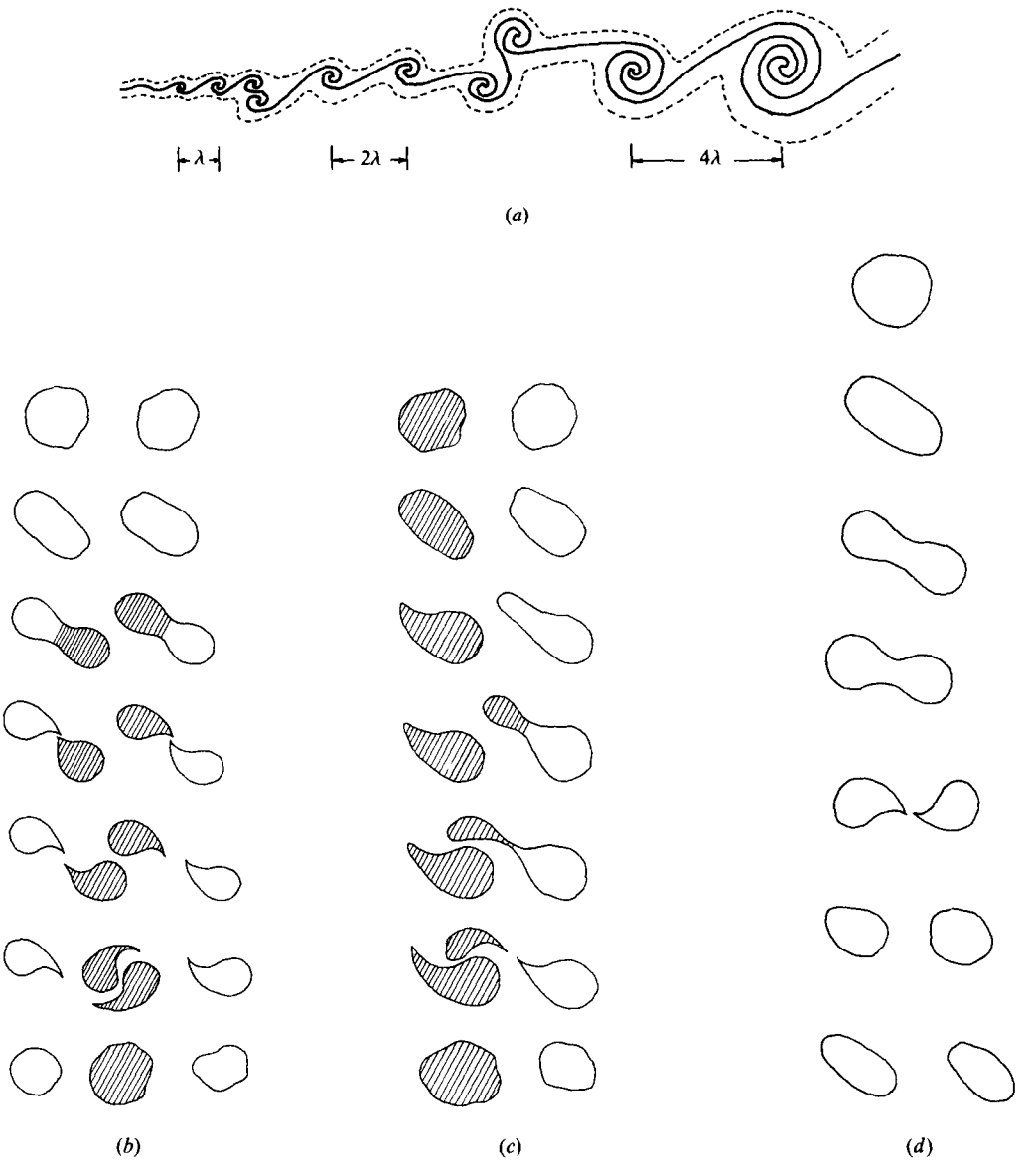

FIGURE 2. Coherent structure interactions in a mixing layer: (*a*) schematic of vortex pairing process; (*b*) schematic of fractional pairing process; (*c*) schematic of partial pairing process; (*d*) schematic of tearing process.

We re-emphasize that a coherent structure by our definition is a statistical entity resulting from the phase-aligned ensemble average of a large number of realizations (i.e. data records) containing the structure. That is, it is not necessarily observable instantaneously or individually, as it is buried in a realization or picture, especially in a fully turbulent flow; it is the (underlying) common denominator of many realizations containing the structures of the same age and mode. Thus one cannot visualize a coherent structure in a turbulent flow. One can recognize large-scale motions, which should perhaps be called flow events or turbulent 'eddy' structures, or simply structures, even though they are loosely called coherent structures by many.

2.5. *Expectations of coherent structures*

Most turbulence researchers have formed opinions about what coherent structures are, how they are formed, and how important they are. Hard facts supporting these expectations are rare. Some facets of these are discussed here.

2.5.1. *Formation of coherent structures*

The formation of (transitional) coherent structures as a result of instability of initially laminar free shear layers or boundary layers is much better understood than their formation in fully turbulent states of shear flows. It seems obvious that these structures form as a result of local instabilities of instantaneous turbulent flows. A number of investigators (Gaster, Wygnanski, Goldstein, Tam and Cimbala, among others) have attempted to explain structure formation in fully turbulent shear flows via *linear* instability of the *time-mean* profile. While it is impressive that some of the theoretically predicted results (for example, lower-order measures of fluctuating quantities) agree well with experimental data (Wygnanski 1985), I find those an insufficient basis for accepting this approach, and have some strong conceptual objections. First, the basic turbulent flow whose instability is sought is itself highly unsteady and mostly consists of nonlinearly interacting large-scale energetic motions. The instability would seem to be a result of these interactions, which are intrinsically nonlinear. Secondly, an instability study of the time-mean profile would be reasonable if the timescales and lengthscales of turbulence were much smaller than those of the instability wave. But the scales of the instantaneous turbulent shear flow are in the same range as those of the instability wave investigated. Thus, it does not seem appropriate to talk about instability of the mean profile if the instability wave never 'sees' the mean profile, or if the average of the flow encountered by a wave during its evolution departs noticeably from the mean profile. Thirdly, it is yet to be shown that to the leading order, the instability of an instantaneous profile is that of the time-mean profile. Finally, even if the profile shape were to remain the same but change in magnitude with time, the instability of a given profile shape when it is unsteady can be quite different from that when it is steady (Davis 1976). From these considerations, it seems clear that a linear instability study of a steady mean profile cannot be relevant to the formation of coherent structures in a fully turbulent shear flow. Newer approaches, perhaps a dynamic stability study of the time-dependent flow, may have to be considered.

2.5.2. *Waves, solitons, strange attractors*

Many (e.g. Tam & Morris 1985) treat coherent structures as waves. There are some who suggest that coherent structures could be viewed as solitons (e.g. Fiedler *et al.* 1980). Since we associate these structures with turbulent fluid mass, it would be inappropriate to view them as waves. Further, since new structures of different scales always result from interactions of coherent structures, they cannot be regarded as solitons. Is the dynamics of a coherent structure described by a strange attractor? Transition in closed flow systems such as Taylor–Couette flow and box convection has shown strange-attractor behaviour (Gollub & Benson 1980; Brandstäter *et al.* 1983; Sano & Sawada 1983), but so far no one has been able to show strange-attractor behaviour in open flows. [Sreenivasan's (private communication, 1985) claim, of a chaotic transition sequence in the cylinder wake, has been brought into question by the recent work of Van Atta & Gharib (private communication), who have shown the apparently chaotic transition frequencies to be related to cylinder vibration modes alone.] While turbulent flows (or for that matter, all flows) have infinite degrees

of freedom, the motion of coherent structures, being large-scale and organized, is likely to be low-dimensional. Also, the Navier–Stokes equation being quadratically nonlinear, like other nonlinear equations depicting strange-attractor-type behaviour, can be expected to have solutions with strange-attractor behaviour (Benjamin private communication, 1985). One can thus expect the time-evolution of a coherent structure to behave as a strange attractor in phase space. Experimental test of this expectation is yet to be made and must await clearer understanding of spatial chaos.

2.5.3. *Vortex dynamics*

The attractiveness of coherent vorticity as the identifier of coherent structures lies not only in our intuitive perception of an organized motion in a turbulent flow being a vortical entity, but also in the general expectation that structure evolution and interaction can be explained via the fairly well-developed theory of vortex dynamics. We need to assess these expectations. Turbulent flow structures are of complex shape, and their interactions are affected by viscosity. On the other hand, most of our notions about vortex dynamics, vortex interactions, and topology of vortical flows (Saffman & Baker 1979; Hunt 1973, 1985; Perry & Chong 1982; Moffatt 1985) are based on Euler flows and vortex filaments of simple geometries (Widnall, Bliss & Tsai 1974; Saffman 1978; Takaki & Hussain 1984). Apart from the complexity of vorticity measurements in a random three-dimensional structure, interpretation of coherent structures via vortex dynamics is difficult. Even if three-dimensionality and viscous effects are ignored, there are problems. For example, Biot–Savart's law applies to instantaneous motions of line (or slender) vortices, and it cannot be applied strictly to the coherent vorticity field to explain the motion of an 'ensemble-averaged vortex' in a turbulent flow. Similarly, the evolution of coherent vorticity cannot be derived by applying the vorticity equation to the coherent flow field alone. In fact, it appears that the principal contribution to coherent vorticity comes from the incoherent field; see Appendix B.

2.5.4. *Other expectations*

Many researchers expect coherent structure to be: (i) quasi-deterministic, (ii) dominant in turbulence phenomena, (iii) long-lived, and (iv) quasi-periodic. It is obvious why these attributes would make coherent structures highly attractive modules of shear flow turbulence. Our experience with coherent structures in different flows enables us to make specific comments about these expectations. Coherent structures are not necessarily long-lived. Their survival distance decreases with increasing Reynolds number. The survival time is typically of the order of the structure turnover time (Hussain & Clark 1981). This observation seems at variance also with the expectation that coherent structures should be characterized by high helicity, which in turn implies relatively long lifetimes (discussed in §4.4). Except in the case of flow resonance or periodic excitation, coherent structures are neither periodic nor quasi-periodic. In some transitional flows such as jets and shear layers, the roll-up of new structures is triggered by feedback from previously formed structures downstream. Thus, quasi-periodicity in transitional regions is not unexpected. Similar feedback is also at play in sustained pairings at nearly the same location in near fields of jets and shear layers. In fully developed turbulent shear flows, there is no reason for the structures or their interactions to be even quasi-periodic. However, it has been found that structures in fully turbulent states occur periodically in patches which, of course, occur randomly (Townsend 1979; Mumford 1982, 1983; Tso 1983). No explanation for this has been given or is apparent.

These claims or expectations about coherent structures have profound implications

and clearly deserve careful scrutiny. We have addressed these claims in our studies of coherent structures in a number of free shear flows. These efforts, though highly painstaking and time-consuming, have proved worthwhile. Our results show that some of the claims about coherent structures need to be moderated. In particular, at least in fully turbulent flows, incoherent turbulence is comparable in importance to coherent structures, and its role in turbulence phenomena cannot be ignored; see also Hussain (1983*a*).

The coherent-structures approach is not a passing phase of the 'rise and fall of ideas in turbulence' (Liepmann 1979), but is here to stay, perhaps with decreased fanfare in the future, which is to be expected. Since it now appears that coherent structures are characteristic features of (perhaps all) turbulent shear flows, understanding of these structures is very important. This understanding should cover the descriptions of the topography of the structures as well as their dynamical significance, including the distributions of structure properties over the spatial extent of the structures. In addition, a number of technological pay-offs may result from manipulation and control of coherent structures, the success of such efforts being dependent on the understanding of the physics of coherent structures. Entrainment, mixing, heat transfer, combustion, chemical reaction, drag and aerodynamic noise generation are fields in which better understanding of coherent structures should produce substantial technological benefits. Some of these aspects will be addressed in §5.

3. Eduction of coherent structures

3.1. *Eduction philosophy*

The eduction process in principle consists of the following steps: (i) deduce a feature of a relevant signal which can uniquely denote passing structures; (ii) select a mode (typically the preferred mode) and a parameter size, and accept signals containing structures of the chosen mode and parameter size; (iii) phase-align (i.e. align in both space and time (or age)) the accepted realizations and obtain their ensemble average (i.e. phase average); (iv) refine the phase average by further discarding the undesirable realizations; and (v) extract the departure of each finally accepted instantaneous realization from the final phase average and compute incoherent turbulence measures.

Since mode identification can only follow structure eduction, which in turn must depend on the choice of the mode and parameter size, eduction of coherent structures in fully turbulent flows is intrinsically iterative. Even after a mode and a parameter size have been selected through some iteration, further iteration via refinement (step (iv)) is necessary. It should be obvious from these steps that eduction of coherent structures is a sophisticated art depending on the imagination (hence prejudice!) of the researcher. This is a well-known dilemma: prejudice which can produce potentially biased or misleading results is also necessary for the success in the eduction of coherent structures in fully turbulent shear flows. Of course, the researcher must ensure that the final phase-averaged structure is based on an adequate number of realizations, and that the eduction process converges to the appropriate preferred mode and not to a freak mode.

3.1.1. *Earlier eduction schemes*

Coherent structures may vary from flow to flow. A flow may have a few preferred modes. In some cases, the same flow may have different preferred modes in different regions. For example, the preferred mode in the axisymmetric jet is toroidal in the near field, but appears to be helical in the far field. When a unique preferred mode

exists, structure eduction can be simplified by exciting the flow at that mode (if such excitation is possible) and educing the structure with a single (cross-wire) probe using phase-locked measurements. Some early studies utilized the periodicity of the structures for their eduction by a single sensor. For example, controlled sinusoidal excitation was used to educe coherent structures at different phases during pairing (Hussain & Zaman 1980) and to educe the preferred mode structure (Hussain & Zaman 1981) in the axisymmetric jet near field. The near periodicity of the vortex-shedding process was utilized by Cantwell & Coles (1983) to educe the structure in the near-turbulent wake of a circular cylinder.

It is necessary to emphasize that in the case of structure evolution in a turbulent environment, there is jitter both in the initiation of successive structures and in the structure trajectory or evolution. In order to reduce both jitters, the conditional sampling for eduction should be triggered not by the excitation signal or a signal denoting structure initiation, but by a local flow signal capturing footprints of structures at the measurement station. Hussain & Zaman (1980, 1981) triggered the sampling on the jet centreline velocity signal at the measurement station. On the other hand, Cantwell & Coles (1983) triggered the sampling of cylinder wake structures on a pressure signal from the shedding cylinder; this removed the initiation jitter but not the structure evolution jitter. For this reason, their data must have been significantly affected by smearing, which increases with increasing downstream distance from the structure initiation point.

Such smearing can be removed easily if the captured structure signatures are appropriately aligned with respect to each other before the ensemble average is computed. In a turbulent environment, iterative cross-correlation of each realization (i.e. signal of a flow variable) with an ensemble average seems to be the obvious choice for alignment of successive realizations. An example is the organized turbulent structure (such as a boundary-layer spot or a free shear-layer spot) initiated via suction or spark and educed further downstream (Zilberman, Wygnanski & Kaplan 1977; Cantwell, Coles & Dimotakis 1978; Sokolov *et al.* 1980).

3.1.2. *Excited vs. natural structures*

The relevance of an excited structure to natural or unexcited structures has been questioned often. In reality, all flows are excited, as disturbance-free flow is impossible to produce (Hussain 1980). Thus a discussion about natural and excited flows is really about structures produced by uncontrolled and controlled excitations. When the excitation amplitude is small (i.e. in the linear range), an arbitrary broadband disturbance can trigger the formation of only the most unstable mode, the so-called natural structures. The evolution of an excited structure cannot differ largely from that of a 'natural' structure in the same configuration, because the governing equation and boundary conditions are the same. Excitation thus merely paces the initiation of the natural structures at periodic intervals. Our earlier claim that small-amplitude excitation at the preferred mode produced only natural structures was tested and validated: the topographical details of structures for excited and unexcited jets were found to be nearly identical when the excitation amplitude is in the linear range. (The unexcited structure was educed using the generic eduction scheme discussed in §3.4 and compared with the excited structure educed by phase-locked measurements.) When the excitation amplitude was large, the structures were different, as is expected (Zaman & Hussain 1984). Depending on its frequency and amplitude, an excitation can significantly alter structure interactions; such interactions are of both scientific and technological interest (see §5). In

the following, we briefly review some examples of eduction under controlled excitation, not only to demonstrate the success of eduction, but also to present some structure data which will be discussed later (see §4.3). Lack of space prevents us from dwelling on the specific details of the flow physics.

3.2. *Examples of eduction using controlled excitation*

3.2.1. *Circular jet*

Two examples of coherent-structure eduction using controlled excitation are those of stable vortex pairing and preferred modes in the axisymmetric jet. Both studies involved excitation at 2% of the exit velocity in a low-speed air-flow facility consisting of two settling chambers in series. Plane-wave excitation of the jet was introduced by inducing organ-pipe resonance of the settling chambers with the help of a loudspeaker attached to the first settling chamber. Measurements at the nozzle exit confirmed axisymmetry of the mean and turbulent flow fields, and spectra showed no strong residual frequency component. This ensured that the flow was clean; the exit broadband total turbulence level was less than 0.001; the previously reported value of turbulence level was higher because of the inclusion of linearizer noise. It should be emphasized that whether a jet flow can be characterized as 'clean' or not depends more on the presence of sharp spectral peaks than on the r.m.s. fluctuation level in the exit-plane velocity signal. That is, distinguishable sharp spectral peaks even at a low free-stream turbulence level may suggest a more 'unclean' flow than the case of higher free-stream turbulence level without any strong spectral peak. In either case, it is the amplitude of the spectrum in the range of unstable frequencies, rather than the total r.m.s. value, which should be of concern. Jet studies should report the initial condition: the mean and turbulence characteristics of the exit boundary layers and, especially, the free-stream turbulence spectrum. The importance of the initial conditions in the evolution of jets and shear layers has been emphasized before (Bradshaw 1966; Foss 1977; Hussain 1980).

Excitation at $St_D(\equiv fD/U_e) = 0.85$ produced stable vortex pairing, i.e. successive pairings always occurred at the same spatial station at regular intervals, thus allowing eduction via phase-locked measurements; f_p is the excitation frequency, U_e is the jet exit velocity and D is the jet diameter. The acceptance of successive events was triggered by the periodic 'signature' of the event itself, derived from the velocity signal on the jet centreline at the measurement point. Data (figures 3*a–g*) were taken in a 7.6 cm air jet at the Reynolds number of 3.2×10^4 and at the instant when pairing occurred in the jet column mode at $x \approx 1.75D$. Note that an earlier phase of the structure during roll-up and two later stages after pairing were also captured. Figures 3(*a–f*) show the contours of coherent spanwise vorticity, coherent Reynolds stress, incoherent Reynolds stress, incoherent turbulence intensities, and coherent production of incoherent turbulence. The structure details have been discussed by Hussain & Zaman (1980). Figure 3(*g*) shows the time-average production and will be discussed in §4.2.

The preferred mode of the axisymmetric jet excited at $St_D = 0.3$ at an excitation amplitude $u_f'/U_e = 2\%$, was studied over a range of Reynolds number and initial condition (i.e. laminar or turbulent exit boundary layer). Figures 4(*a–e*) show the contours of coherent azimuthal vorticity, incoherent turbulence intensities and Reynolds stress, and coherent production for the axisymmetric jet preferred mode. These data are from a 7.62 cm tripped jet at a Reynolds number of $Re_D = 110000$. The data are essentially the same for a wide range of the Reynolds number and initial condition and have been discussed by Hussain & Zaman (1981). The implications of these data are discussed in §4.3.

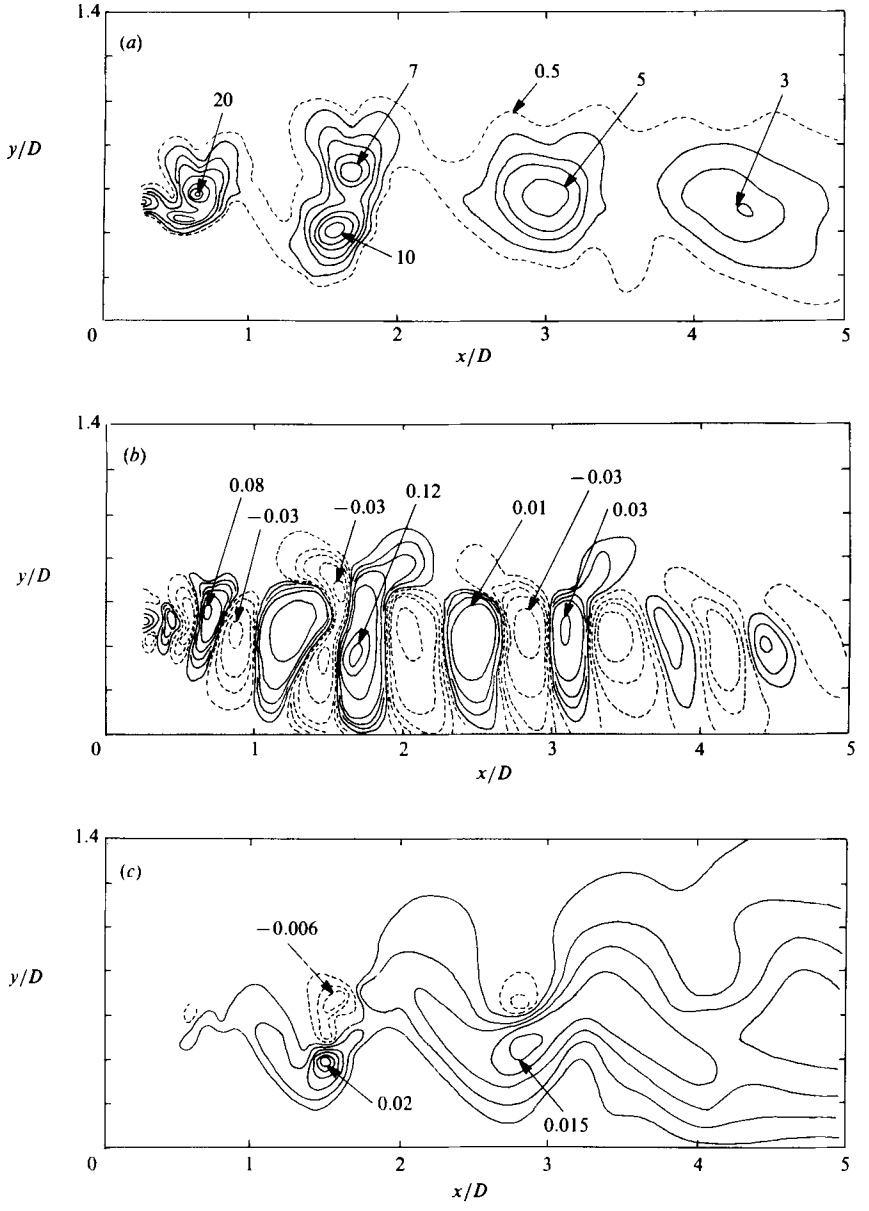

FIGURE 3 (*a–c*). For caption see p. 319.

3.2.2. *Excited elliptic jet*

Stable pairing and preferred modes of elliptic jets were educed following the same excitation and eduction scheme used for circular jets. For excitation effects on elliptic jets see §5.2. Figures 5(*a*, *b*) show the contours of vorticity and production for the preferred mode coherent structure in the two planes of symmetry. These data were taken in a 2:1 jet at the exit speed $U_e = 10$ ms^{-1} corresponding to the jet Reynolds number of $Re_{D_e} = 3.5 \times 10^5$ (based on the effective diameter D_e defined in §5.2). In spite of the differences between the circular and elliptic jets, both in time-mean and instantaneous flow dynamics, there is a great deal of similarity between the contours of structure properties in the two flows.

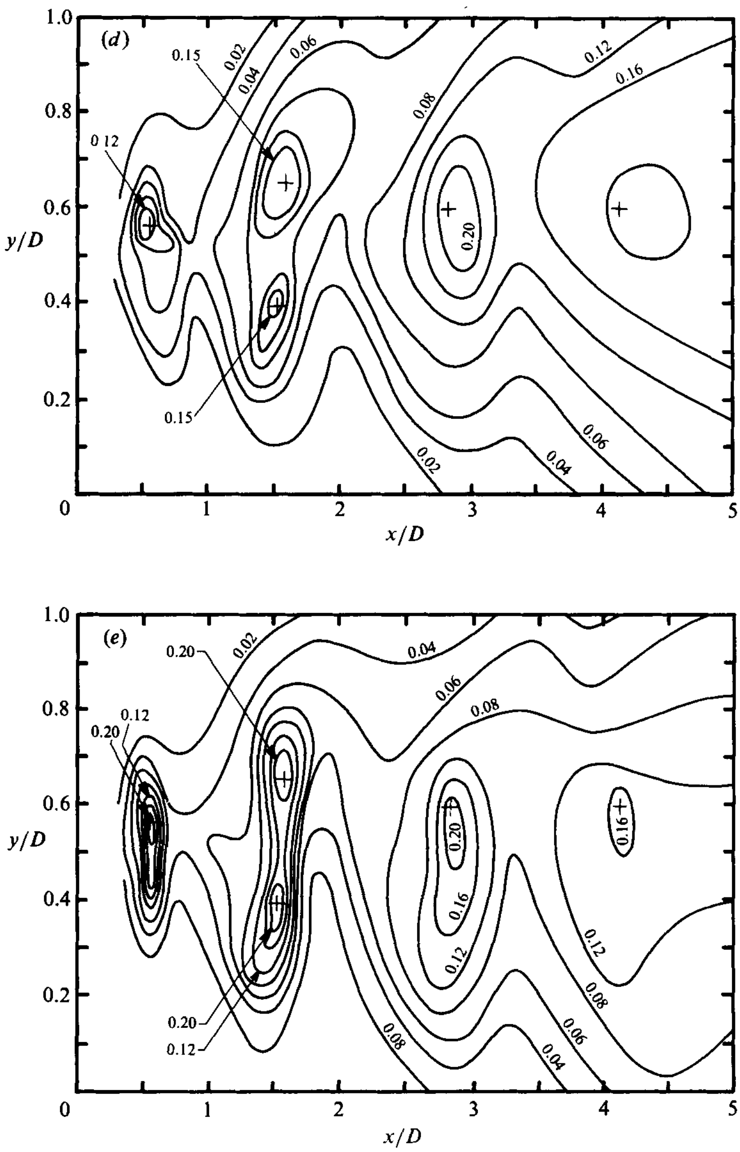

FIGURE 3 (d,e). For caption see facing page.

3.3. *Eduction in fully turbulent flows*

Early eduction efforts were based on a local detection signal. Browand & Weidman (1976) employed longitudinal velocity signals from the edges of a mixing layer to extract the vorticity contours for a pairing stage of the structures. A reference velocity signal u_r from the high-speed edge of the mixing layer has been used for triggering structure eduction by Zaman & Hussain (1984) in a turbulent axisymmetric mixing layer, and by Hussain & Zaman (1985) in a plane mixing layer originating from a fully turbulent boundary layer. Using flow visualization in the near field of a circular jet, peaks in u_r were related to passages of vortical structures. The eduction scheme was first developed in the turbulent axisymmetric mixing layer after considering various options, and was found to be the optimum for the plane mixing

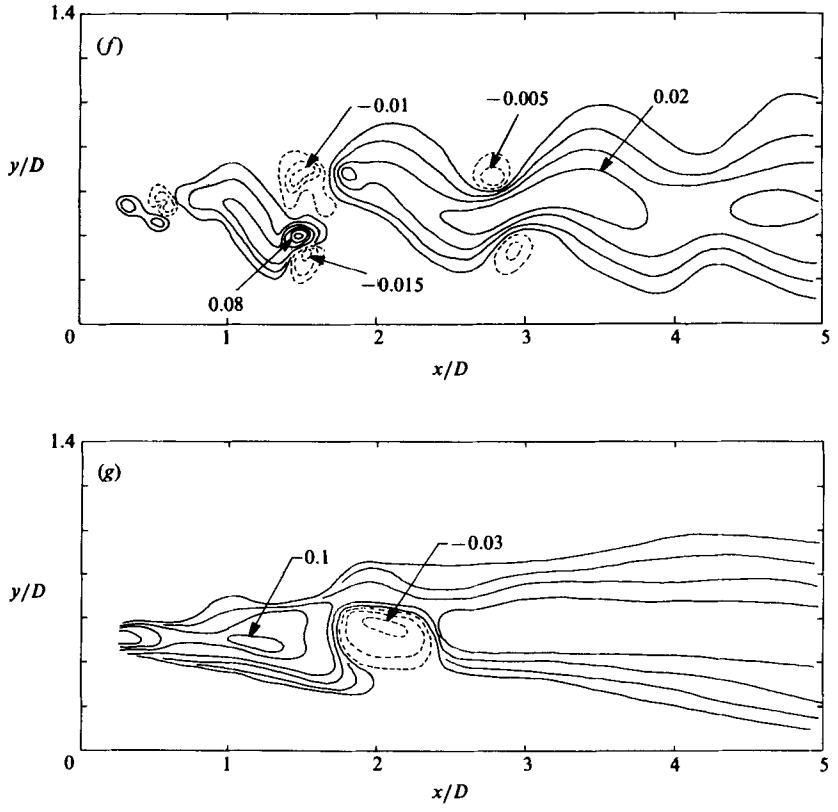

FIGURE 3. Coherent structures in the near field of an axisymmetric jet at the instant of pairing in the jet column mode at $x \approx 1.75D$: (*a*) contours of coherent spanwise vorticity $\langle \Omega \rangle$; numbers denote vorticity non-dimensionalized by the excitation frequency f_p; (*b*) contours of coherent Reynolds stress $\langle u_c v_c \rangle / U_e^2$; (*c*) contours of incoherent Reynolds stress $-\langle u_r v_r \rangle / U_e^2$; (*d*) contours of longitudinal incoherent turbulence intensity $\langle u_r^2 \rangle^{\frac{1}{2}} / U_e$; (*e*) contours of transverse incoherent turbulence intensity $\langle v_r^2 \rangle^{\frac{1}{2}} / U_e$; (*f*) contours of coherent shear production $\langle P_s \rangle / (f_p U_e^2)$; (*g*) contours of time-averaged production $P/(f_p U_e^2)$; note the 'negative production' in (*g*) induced by excitation; U_e is the jet exit velocity.

layer also. Data from the measurement probe were accepted whenever a sharp peak in u_r exceeded a set level.

Even though fairly successful, eduction based on a trigger using a local 'footprint' signal from outside the flow has some constraints. Such a 'footprint' signal cannot unambiguously discriminate between structures of different strengths, sizes, shapes, etc. For example, there is no way to determine if a recorded signal is from a weak structure near the probe or from a stronger structure farther away from the probe. Secondly, such a footprint signal approach cannot be used for eduction of structures in turbulent pipe or channel flow or in the inner layer of a turbulent boundary layer. In these flows, as well as in situations like fully developed turbulent jets or wakes, this scheme will not be effective because sharp, identifiable characteristic peaks do not occur in reference signals in these flows. In such situations, it is preferable to base the trigger on the measurement signal itself, so that structure detection and classification are unambiguous. An eduction scheme developed this way would be effective in all possible flow situations such as transitional, resonant, excited, or fully

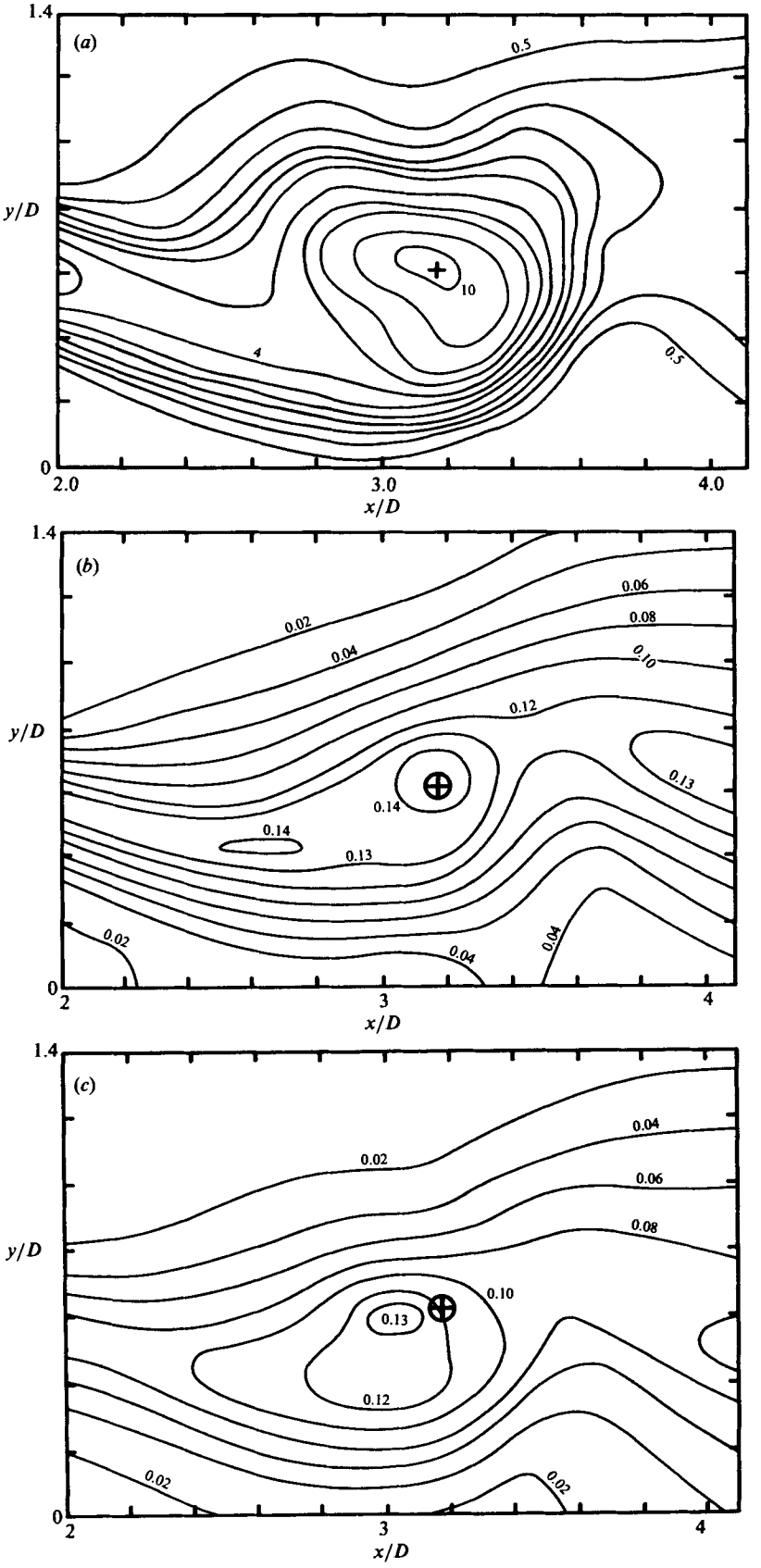

FIGURE 4 (*a–c*). For caption see facing page.

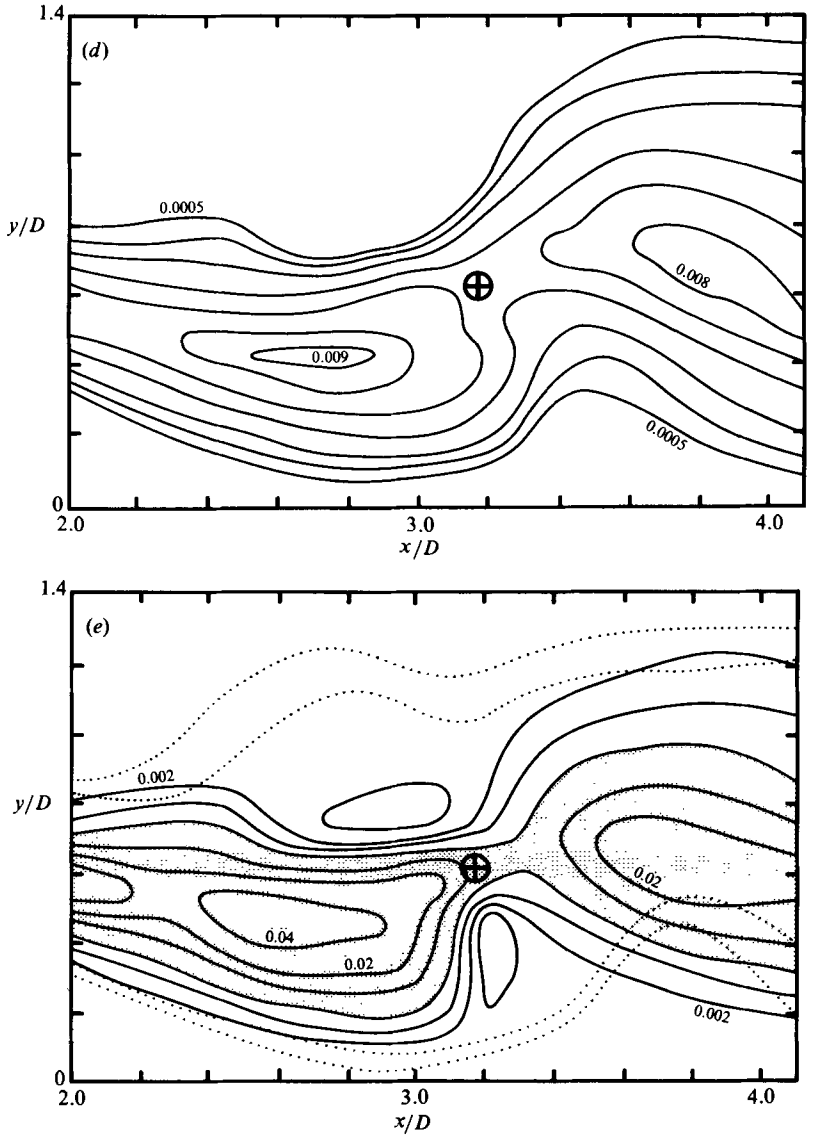

FIGURE 4. Contours of axisymmetric jet preferred mode structure at $Re_D = 110000$: (*a*) coherent azimuthal vorticity $\langle \Omega \rangle / f_p$; (*b*) incoherent longitudinal turbulence intensity $\langle u_r^2 \rangle^{\frac{1}{2}} / U_e$; (*c*) incoherent transverse turbulent intensity $\langle v_r^2 \rangle^{\frac{1}{2}} / U_e$: (*d*) incoherent Reynolds stress $-\langle u_r v_r \rangle / U_e^2$; (*e*) coherent production $\langle P \rangle / (f_p U_e^2)$. The jet is weakly excited at $St_D = 0.3$.

turbulent; it will not require a reference signal and will be free from the constraints discussed above. In the following, we discuss such a scheme, developed and successfully used in our laboratory.

3.4. *A general-purpose eduction scheme*

On the basis of our definition of coherent structures, we feel that the trigger for structure eduction should be based on the instantaneous vorticity signal. The measurement of the instantaneous total vorticity vector being extremely hard, one component of vorticity is a reasonable compromise. Also, since coherent structures

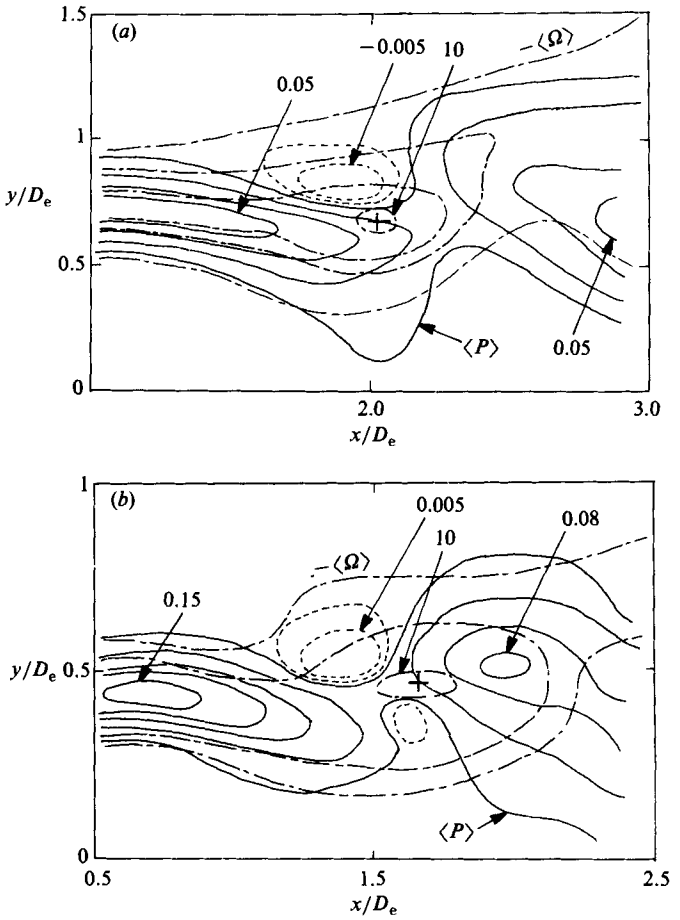

FIGURE 5. Contours of elliptic jet preferred mode structure: coherent vorticity $\langle\Omega\rangle/f_p$ (——) and coherent production $\langle P\rangle/(f_p\, U_e^2)$ (solid and dashed lines) for (*a*) major axis; (*b*) minor axis. Dashed contours denote negative production.

are large-scale, vorticity signals can be smoothed so that instants of occurrence of large-scale vorticity-bearing flow events can be detected.

In principle, a three-dimensional array of fast-response vorticity sensors should be used for structure eduction. However, one must consider probe interference, cost and limitations of present measurement technology (including data sampling and transfer rates of even the fastest computers). These considerations forced us to settle for a simple detection scheme involving smoothed vorticity contours in one plane only. Since in turbulent shear flows spanwise vorticity is expected to be dominant on the average, the eduction scheme is based on the spanwise vorticity. This scheme involves recording signals from an array of cross-wires, which are separated in the transverse direction and thus can provide the instantaneous vorticity in the spanwise (i.e. (x, y)-) plane.

3.4.1. *The eduction procedure*

For a transverse array of cross-wires with a separation of Δy between adjacent probes, the use of Taylor's hypothesis, i.e. $\partial/\partial t = -U_c\,\partial/\partial x$, is unavoidable in the computation of spanwise vorticity ω. This suffers from two constraints: validity of

the hypothesis and choice of the U_c value. Even though it is widely held that Taylor's hypothesis is inapplicable to turbulent shear flows, we have found that the hypothesis is valid for structures not in the process of tearing or pairing and that the true structure advection velocity should be used for U_c (Zaman & Hussain 1981). The measurement of U_c itself is a challenging chore. The typical space–time correlation of velocity provides only a qualitative measure of U_c, but is averaged over various motions (which are not all coherent structures). Such measurements are not only unrepresentative of the physics, but can be misleading. For example, such measurements give large variation (as much as threefold) in the advection velocity across the mixing layer of a circular jet (Bradshaw *et al.* 1964; Ko & Davies 1971; Lau & Fisher 1975; Lau 1979). This well-documented, but striking observation should be evidence enough of the limitation of the correlation measurements [but can be reconciled by the occurrence of frequent tearing, and partial and fractional pairings in the mixing layer, as discussed by Hussain & Clark (1981)]. We have found that the wavenumber-celerity spectrum (Clark 1979) provides a fairly accurate measure of the dominant structure velocity. The most accurate measurement of U_c results from space–time correlation of large-scale vorticity maps, obtained with two rakes of cross-wires separated in the streamwise direction.

In the computation of vorticity, the central difference approximation was used so that an array of N number of cross-wires gave the instantaneous vorticity at $(N-1)$ intermediate locations, i.e. circulations at the regions between neighbouring cross-wires. (In our measurements so far we have had $N = 8$.) The unavoidable smoothing in this process due to finite transverse probe spacing is not a constraint for large-scale structures. In fact, in order to highlight the large-scale structures as well as locate their vorticity peaks, this smoothing is necessary, and we even perform further smoothing by the short-time averaging over a period T_1 centred at each instant t. The choice of T_1 is somewhat arbitrary. Clearly, T_1 should be chosen to be smaller than, but of the same order as, the average time between passages of large-scale structures so that this averaging smooths out the high-frequency (i.e. mostly incoherent) fluctuations but retains the underlying large-scale vorticity. The obvious arbitrariness in the selection of T_1 should be of no concern, as the coherent structure properties are finally extracted directly from the primitive, unsmoothed signals recorded. The smoothing is only a means of detecting coherent structures buried in random signals and identifying the amount of relative shifting required for optimum alignment.

Of the structures which are located at the middle of the rake we limit further selection on the basis of two principal criteria: structure strength, and structure shape and size. That is, we accept structures which are sufficiently strong and of a sufficiently large size. We use the peak (smoothed) vorticity value ω_p as a measure of the structure strength. A judicious choice of the threshold ω_{t1} for the peak vorticity should not only involve a local flow measure but also a study of the structure passage frequency f as a function of ω_{t1}. The local maximum mean shear $S_M = (\partial U/\partial y)_{max}$ seems to be the obvious choice for fixing ω_{t1}. In free shear flows we find that an ω_{t1} value between two and three times the value of S_M is adequate. After detecting structures with peak vorticity values above ω_{t1}, the locations (y, t) of the peaks (i.e. centres) are assigned the coordinates (y_c, t_c). The next step is to specify the structure size. We need to specify the transverse size Δy and require that the smoothed vorticities at $(y_c \pm \Delta y, t_c)$ have the same sign as that at the centre and have values above a threshold ω_{t2}. From a study of the population of structures accepted as a function of Δy subject to the threshold criterion ω_{t2}, a suitable Δy can be chosen. The streamwise extent Δx of each structure centred at t_c can be selected arbitrarily. Accepting short-time

validity of Taylor's hypothesis, i.e. $\Delta x = -U_c \Delta t$, we require that the smoothed vorticities at $(y_c, t_c \pm \Delta x/U_c)$ should be higher than ω_{t_2} and also be of the same sign as that at the centre. We chose $\Delta x \approx \Delta y$; this choice is reasonable because we do not expect the coherent structure to be highly elongated. However, the size criterion is chosen conservatively enough that structures of various sectional shapes will still survive through the eduction scheme, and the eduction scheme will sift out the dominant structure shape.

Note that we have applied the transverse size criterion only at t_c. A more rigorous, but time consuming, alternative will be to take short-time correlation between smoothed vorticity signals at $y_c \pm \Delta y$ and require that these two signals are well correlated over a period $\Delta\tau$ around t_c; this condition has been used in our laboratory by Tso (1983) for eduction in the fully developed turbulent region of a circular jet (see §3.5.2).

3.4.2. *Phase average*

Large-scale structures are accepted only when all criteria mentioned above are satisfied so that weaker, smaller, fragmented, distorted or transversely shifted structures are discarded from the ensemble average. With the structure centre as a phase (i.e. time) reference, accepted structures are then relatively aligned with respect to their centres (y_c, t_c) and ensemble-averaged. This is the zeroth-iteration ensemble average. Since smoothed vorticity peaks may not be sharp, may not be clearly identified, or may not even be the true structure centres, it is necessary to refine further the alignment process outlined above in an attempt to sharpen the educed structure details and minimize the smearing effect of structure property dispersion on the educed structure. This refinement is achieved by taking the cross-correlation of individual structure vorticity and the zeroth-iteration ensemble average vorticity. Each realization is then relatively re-aligned (i.e. t_c is shifted) by the time shift of the peak correlation. The resulting ensemble average of the realigned structures is the first-iteration ensemble average. This alignment process can be iterated until convergence is achieved.

During the iteration process, structures requiring excessive shifts are discarded. As a next step in the improvement of eduction, further rejection is carried out by discarding weak structures. That is, additional structures are discarded if the vorticity correlation peak value is lower than a specified value. These enhancement procedures were adopted in order to sharpen further the educed structure features.

Note that smoothed vorticity was used to detect acceptable structures and to determine time shifts for their optimal relative alignment. Once the structures (that meet the selection criteria) are identified and the corresponding necessary time shifts (or true structure centres) are known, the smoothed signals have served their purpose and are then *discarded*; only *unsmoothed* (raw) signals (around the revised structure centres) are used for ensemble-averaging in order to educe the structure, and these are optimally aligned before the average is computed. We also re-emphasize that the eduction scheme does not create an artificial structure, but merely helps select preferred natural structures and sharpen the structure details. Without a rigorous scheme like this, the educed structure will be excessively smeared and will reveal very little flow physics. The final ensemble average is the expected phase average.

3.5. *Applications of the eduction scheme*

The eduction scheme explained above has been employed to educe coherent structures in the turbulent cylinder wake, the fully developed region of the turbulent axisym-

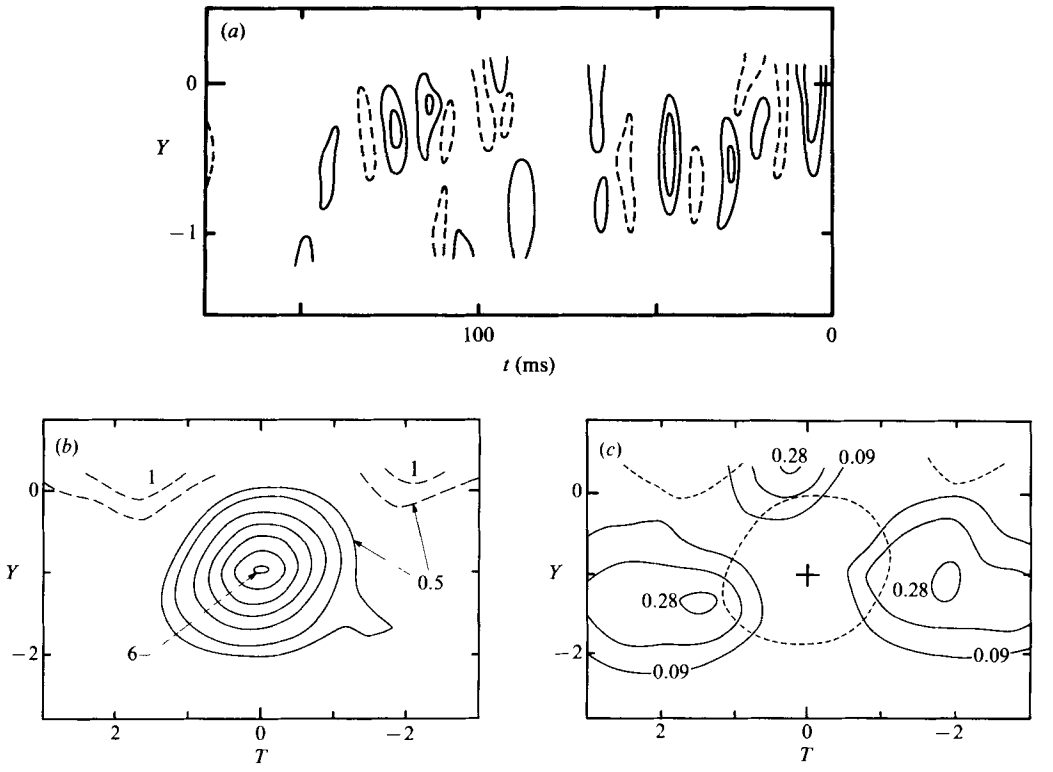

FIGURE 6. Coherent structure in the turbulent wake of a cylinder at $x/d = 40$: (*a*) contours of smoothed instantaneous spanwise vorticity ω/S_M; (*b*) ensemble-averaged spanwise vorticity $\langle\Omega\rangle/S_M$; (*c*) contours of coherent production $\langle P\rangle/(U_0^2 S_M) \times 10^2$; U_0 is the free-stream velocity; $T = tU_c/d$.

metric jet, and the plane mixing layer by using a transverse rake of cross-wires. It is clear that the same scheme can be employed for eduction using other measurement techniques such as scanning LDA, particle displacement velocimetry and digital image processing as well as using direct numerical simulation. We will discuss first hot-wire studies and then the eduction from direct numerical simulation of turbulent flows.

3.5.1. *Fully turbulent plane wakes*

We have applied this scheme to the case of the fully turbulent wake (in air) of a rigid circular cylinder of diameter $d = 2.7$ cm at the Reynolds number $Re_d = 1.3 \times 10^4$ (Hayakawa & Hussain 1985). Figure 6 (*a*) shows contours of smoothed instantaneous spanwise vorticity at $x/d = 40$. If time t is transformed to streamwise distance x by assuming $x = -U_c t$, the streamwise coordinate here is compressed 5 times to include more structures. The contour levels are non-dimensionalized by the maximum mean shear $S_M = (\partial U/\partial y)_{max}$. The contours of the two vorticity signs are denoted by solid and broken lines. The vortices, which are shed almost identically, are extremely irregular at $x = 40d$. There are frequent excursions of vortices across the wake centreline ($Y \equiv y/d = 0$) and smaller and intermediate size contours indicate significant tearing. Note that most structures are located much closer to the wake centreline than the half width of the wake. While the vortices are shed alternately and are of equal strength, the adjacent vortices further downstream are not of opposite sign, and their strengths vary widely. Thus, if eduction is triggered

on the initial vortex-shedding signal, the educed structures will suffer from significant smearing. Such smearing appears to be a major drawback of the results of Cantwell & Coles (1983).

We chose $\omega_{t1} = 3S_M, \omega_{t2} = 0.5\,S_M, \Delta y = 0.4b$, where b is the local wake half-width. In the wake, we found that 60 % of the detected structures were satisfactorily aligned in the zeroth iteration and 90 % of the structures aligned after first iteration. Ensemble-averaged spanwise vorticity contours at $x = 40d$ are shown in figure 6(*b*). The aligned structure (below the centreline) is shown by solid lines and the two adjacent vortices of the opposite sign are shown by broken lines. Coordinates are non-dimensionalized by the structure convection velocity U_c and the cylinder diameter d. The lower contour level values for the broken-line contours are due to jitter relative to the alignment point. The corresponding contours of turbulence production $\langle P \rangle$ are shown in figure 6(*c*). Note that turbulence production at the structure centre is very small, but is larger in the upstream and downstream directions, being the maximum at the saddle on either side.

3.5.2. *Self-preserving region of circular jets*

Spurred by our expectation that coherent structures are characteristic features of all turbulent shear flows, we studied structures in the fully developed state of a turbulent circular jet. In this particular case we used a radial rake of 7 cross-wires; two single hot-wires were placed at the same station but displaced azimuthally by 90° on either side of the rake in order to identify the azimuthal mode of structures detected. This study has been carried out at $x/D = 50$ and 100 in an axisymmetric air jet at $Re_D = 10^5$. The probe configuration enabled us to identify the modes ($m = 0, +1, -1, +2, -2$) of the structures. Results briefly discussed here are based on ensemble averages of 400 realizations. The robustness of the eduction scheme was confirmed by the facts that contour details of structure properties changed very little between 200 and 800 realizations, that left-handed and right-handed helical modes (i.e. $m = +1$ and $m = -1$) were detected with equal probability and their properties were found to be identical (thus confirming the lack of any bias in the facility), and that structure details at $x/d = 50$ and 100 were virtually identical (thus suggesting the achievement of equilibrium of the educed coherent structures). The modes 0, 1 and 2 are found to occur at the local St_D values of about 0.5, 0.41 and 0.54, respectively; these numbers have fairly large uncertainties. Also, the $m = 0, 1, 2$ modes were found to occur about 2 %, 12 % and 3 % of the total time, indicating $m = 1$ to be the dominant mode.

Figures 7(*a–c*) show the contours of the azimuthal coherent vorticity, transverse coherent velocity, and coherent production for the $m = +1$ mode. The structure front (i.e. downstream side) is considerably more active than the back (i.e. upstream side). The radial outward ejection of the fluid at the front, which is much stronger than the radial ingestion of the ambient fluid at the back of the coherent structure, seems to be the primary mechanism of jet mixing – a conclusion also reached on the basis of earlier flow visualization (Hussain & Clark 1981). Note that the active fronts revealed by our data appear to be consistent with to the gaps revealed by the flow visualization pictures of Dimotakis, Miake-Lye & Papantoniou (1983). The incursions of non-turbulent ambient fluid to the jet centreline should not be surprising; thus the intermittency value on the jet centreline can obviously be less than 1 even though most experimenters have set it to 1 (see, for example, Wygnanski & Fiedler 1969). However, as we have frequently warned, one must also be careful about taking the flow visualization pictures too seriously. Further details of the far field of the circular jet have been reported by Tso (1983).

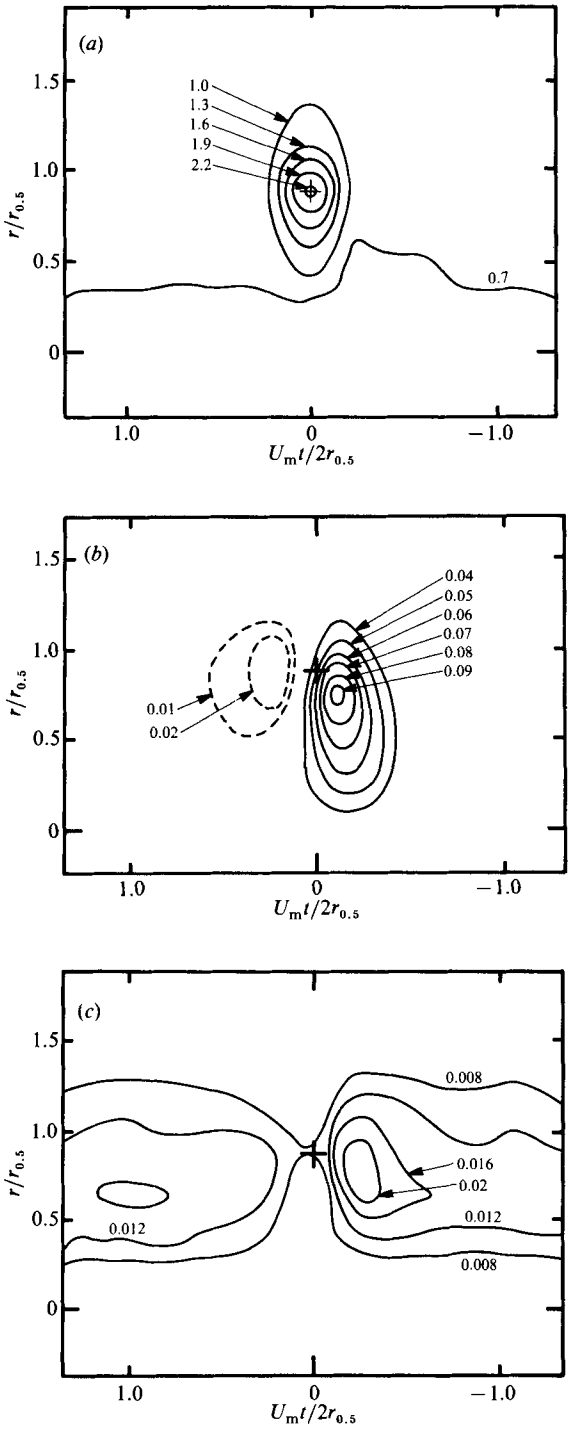

FIGURE 7. Coherent structures in the far-field of the circular jet for the $m = +1$ mode: (*a*) azimuthal coherent vorticity $\langle \Omega \rangle / S_M$; (*b*) transverse coherent velocity v_c/U_c; (*c*) coherent production $\langle P \rangle / (U_c^2 S_M)$. U_c is the local centreline mean velocity. $r_{0.5}$ is the half-velocity radius where mean velocity is half of local maximum velocity U_m.

3.5.3. *Eduction in turbulent mixing layers*

(*a*) *Laboratory experiments.* Exactly the same scheme has been used to educe coherent structures in a fully turbulent plane mixing layer. To eliminate the effects of the initial instability and to focus on coherent structures in the fully developed turbulent region, the study was carried out in a single-stream plane mixing layer originating from a fully developed turbulent boundary layer. Just like a laminar free shear layer, the initially fully turbulent mixing layer also rolls up and then undergoes subsequent evolutions via pairing. We focused our attention on the single structure, not on a pairing stage. The evolution of the structure is complete before $x = 500\theta_e$, beyond which the structure details achieve an equilibrium stage. The flow details have been discussed by Hussain & Zaman (1985); note that the results reported in that paper were based on a trigger derived from a single point at the high-speed edge of the mixing layer.

The present scheme with a transverse rake of 8 cross-wires was applied to educe structure details in the plane mixing layer in the equilibrium range. Figures 8(*a*, *b*) show examples of the recorded time-evolutions of (smoothed) spanwise vorticity maps at $x = 1000\theta_e$ and $2000\theta_e$ respectively. It is interesting to note that, contrary to the impressions one obtains from the Brown–Roshko pictures, the transverse extent of most structures is considerably smaller than the average thickness of the mixing layer. Thus the dominant large-scale structure does not span the average thickness of the layer. The average thickness is larger than the transverse scale because of transverse wandering (figures 8*a*, *b*) and spanwise contortions of the structures. This has been confirmed by recording spanwise vorticity maps in two planes separated in the spanwise direction. Contours of coherent spanwise vorticity, coherent transverse velocity and coherent production at $x = 2000\theta_e$ are shown in figures 8(*c–e*). The turbulence production contours are also consistent with the data discussed for the other cases; i.e. production is maximum at the braid and is very low at the structure centre.

(*b*) *Direct numerical simulation.* We have taken advantage of the capability of supercomputers to understand turbulent shear flows and to extend the capability of laboratory measurement techniques via direct numerical simulation of the complete Navier–Stokes equations, without recourse to subgrid modelling. Some preliminary results of this study have been reported by Metcalfe *et al.* (1986*a*) and further results will be presented soon. Solutions of the Navier–Stokes equations in three spatial dimensions and time have been obtained on a $64 \times 64 \times 64$ grid domain by applying a pseudospectral method with periodic boundary conditions in streamwise and spanwise (x, z) directions and free-slip conditions in the transverse (y) direction (Gottlieb & Orszag 1977; Riley & Metcalfe 1980; Metcalfe *et al.* 1986*b*). The Reynolds number of the flow was kept sufficiently small for all critical scales of motion to be accurately resolved. The mean velocity profile was a hyperbolic tangent profile on which a background, quasi-random, three-dimensional disturbance velocity field was superimposed. Numerical experiments have been performed for an initial condition with random fluctuations superimposed on: a small-amplitude fundamental (Michalke 1965) to induce roll-up; small-amplitude fundamental and subharmonic perturbations to induce one pairing; small-amplitude fundamental, first subharmonic and second subharmonic perturbations to induce two pairings. In addition, in order to focus on the dynamics of ribs (§4.3), one run included additionally a spanwise wave mode (Lin & Corcos 1984) in order to induce well-defined ribs. These flows with initially organized modes correspond to experiments with

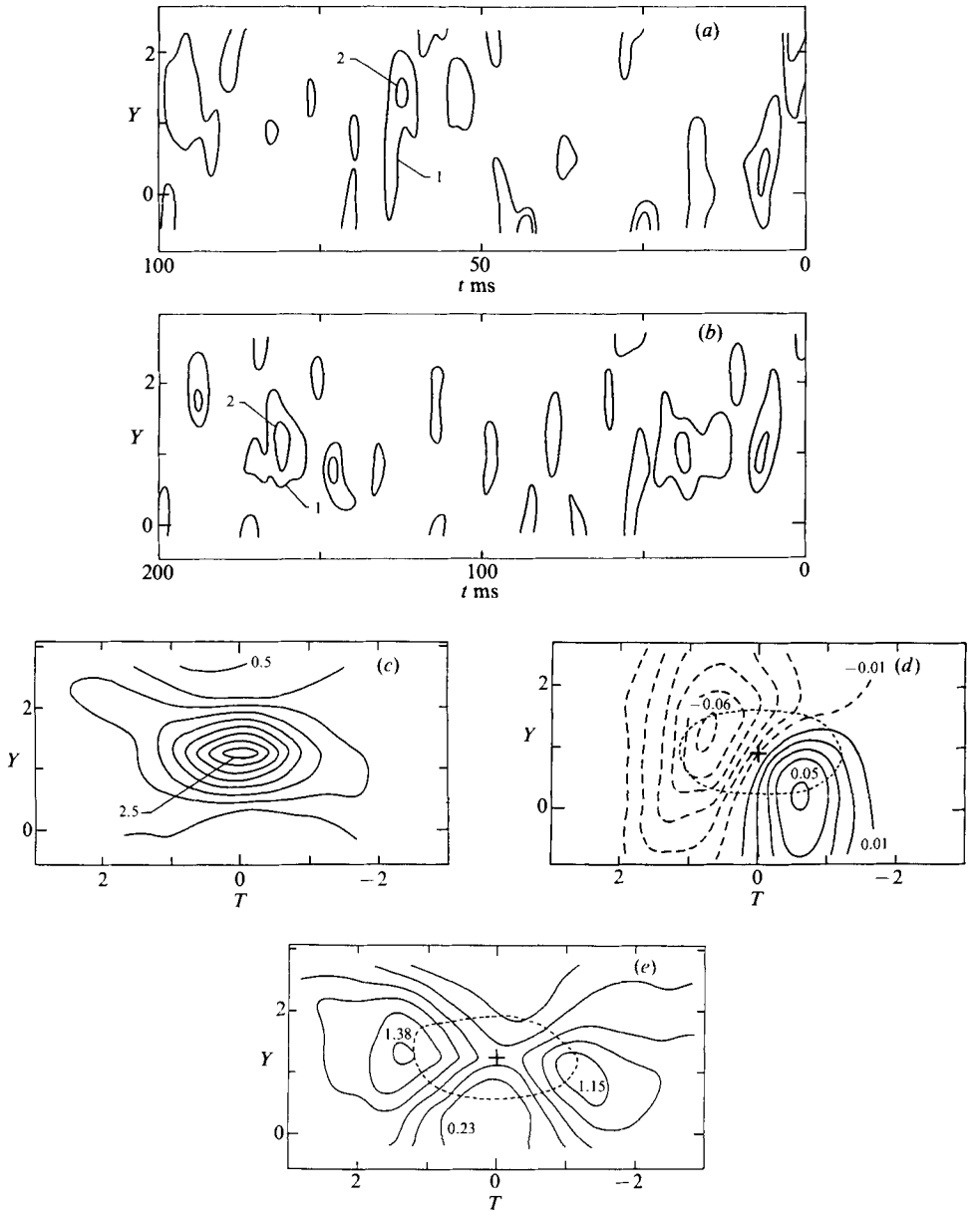

FIGURE 8. Eduction of coherent structure in the fully turbulent plane mixing layer: (*a*, *b*), contours of smoothed spanwise vorticity ω/S_M; $\theta_e = 0.67$ mm; (*c*) spanwise coherent vorticity $\langle\Omega\rangle/S_M$; (*d*), coherent transverse velocity v_c/U_0; (*e*) coherent production $\langle P\rangle/U_0^2 S_M$). U_0 is the high-speed side mean velocity; $U_0 = 12.3$ m/s; $T = tU_0/\theta_e$; $Y = y/\theta$, where θ is the local momentum thickness of the mixing layer.

controlled excitations. As discussed earlier, controlled excitation is particularly preferable for focusing on specific flow events.

There are a number of differences between the laboratory experiments and numerical experiments using spectral methods. The former is evolving in space; the latter is evolving in time, which allows higher Re and better resolution than spatial simulation, but it is less realistic as it uses periodic boundary conditions. Recent

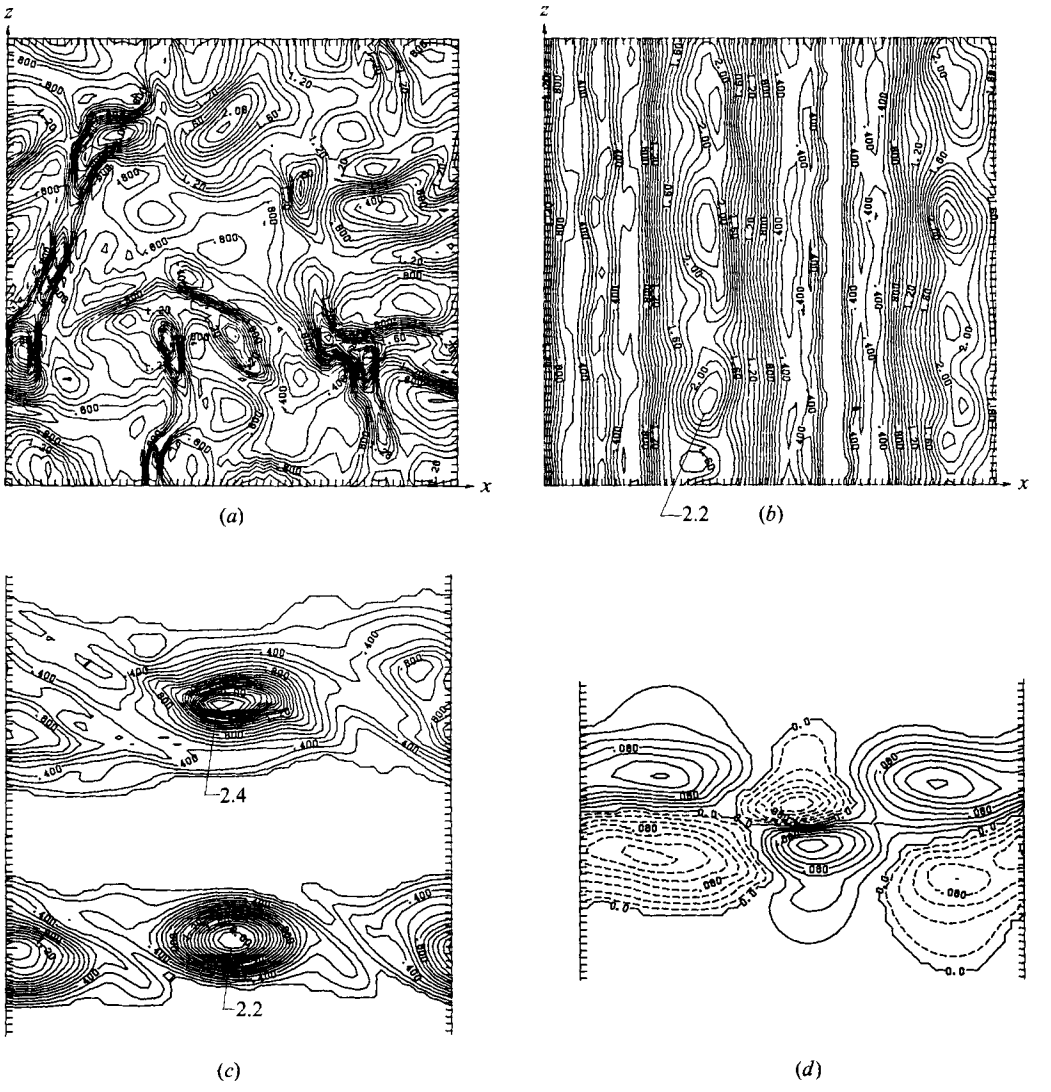

FIGURE 9. Coherent structure characteristics in a plane mixing layer computed by direct numerical simulation: (*a*) contours of instantaneous vorticity ω_z/S_M in the (x, z)-plane at $y = 0$; contour values range from 0 to 2.5 in increments of 0.1; (*b*) same contours as in (*a*) but with small amount of forcing; contour values are in increments of 0.1; (*c*) ensemble average spanwise vorticity $\langle\Omega\rangle/S_M$ contours for cases (*a*) (top) and (*b*) (bottom); contour values in increments of 0.1; (*d*) contours of coherent streamwise velocity u_c/U; contour values are from -0.14 to 0.16 in intervals of 0.02. The velocity difference is $2U$ across the mixing layer.

spatial simulations have successfully used inflow–outflow boundary conditions (e.g. Grinstein, Oran & Boris 1986*a*, *b*). The Reynolds numbers are $Re_\delta \approx 10^5$ and $Re_\lambda \approx 1500$ for the experiment as opposed to $Re_\delta \approx 10^3$ and $Re_\lambda \approx 60$ for the simulation; δ is the local thickness of the mixing layer. The laboratory flow is that from an initially fully developed turbulent boundary layer, and phase averages include selection from many (about 10^4) realizations. The simulation involves uncorrelated random initial disturbances, and multiple realizations (up to 64) are achieved from the same computation by taking data at successive spanwise planes as separate realizations. In spite of these differences, the agreement between experiments and simulations (discussed below) seems impressive.

Figure 9(*a*) shows the contours of instantaneous vorticity ω_z/S_M in the (x, z)-plane at $y = 0$. It is clear that there is no spanwise coherence of structures in the unforced simulation, consistent with our laboratory data. Even a small amount of forcing organizes the structures in the spanwise direction (figure 9*b*). The ensemble average spanwise vorticity contours are shown in figure 9(*c*) for the unexcited (top) and excited (bottom) cases. Note the close correspondence between not only the peak values but also the contour shapes. The contours of coherent streamwise velocity (unexcited case) are shown in figure 9(*d*). Considering the limitations of the two techniques, the agreement with laboratory data (compare figures 8*c* and 9*c*) is very good. Detailed comparison and discussions will be given in a forthcoming paper by Hussain & Metcalfe.

4. Some benefits of the coherent structure concept

The coherent structure approach to turbulence has already produced some benefits. These include understanding of entrainment phenomena, explanation of negative production, insight into the physics of turbulence production (such as roles of ribs and vortex stretching), assessment of turbulent flow topology, and explanations for excitation-induced enhanced mixing, turbulence suppression and noise suppression. We will discuss some of these briefly.

4.1. *Entrainment*

One inference from coherent structures interaction is that entrainment is not just diffusion of vorticity at the turbulent/non-turbulent interface, somewhat like nibbling away of irrotational fluid by a swarm of fine-scale vortices. Entrainment is now believed to be mostly a result of large-scale engulfment of non-vortical fluid due to the Biot–Savart induction of large-scale coherent structures near the interface. Of course, only viscosity can cause true entrainment via diffusion. Once a non-turbulent blob is entrapped within the influence of a coherent structure, the non-turbulent fluid is sheared into thin laminations with increased interface so that (molecular) diffusion of vorticity fluctuations by viscosity can effectively complete the turbulent entrainment process – the process of imparting random, three-dimensional vorticity to irrotational fluid.

4.2. *Negative production*

An understanding of the elusive, so-called phenomenon of 'negative production' or counter-gradient transport of heat and momentum can be obtained via the coherent structures concept. In most turbulent shear flows, the mean velocity gradient and the mean momentum transport by turbulence (i.e. the Reynolds stress, $-\overline{uv}$) retain the same sign across the flow or switch sign together so that their product, i.e. the shear production, remains unchanged in sign. (In coordinates aligned with the free-stream velocity, the time-average production in high-speed shear flows is essentially shear production $\overline{P}_s$, as normal production $\overline{P}_n$ is comparatively small.) The momentum transport is then in accord with the gradient transport hypothesis; i.e. the mean momentum transport by turbulence is down the mean momentum gradient. (As is well recognized now, this kind of gradient transport concept, borrowed from kinetic theory, is not appropriate for turbulent shear flows.) However, in the case of non-symmetric flows such as a wall jet or a channel with the two walls of unequal roughnesses, the zeros of the mean velocity gradient and the Reynolds stress ($-\overline{uv}$) do not coincide. Consequently, there is a (small) region of 'negative production' where the mean momentum transport by turbulence is counter to the mean momentum gradient $\partial U/\partial y$. Even though this does not violate any basic principle and should

not be particularly surprising, this has been the subject of some controversies and investigations (Beguier *et al.* 1977; Hinze 1970; Hanjalic & Launder 1972). It is clear that turbulent heat or mass transfer in shear flows with non-symmetric mean temperature or mean concentration profiles should also have regions of counter-gradient heat or mass transport.

Our studies of coherent structures have provided specific examples of negative turbulence production (Hussain & Zaman 1980, 1985) and direct explanations for negative production in terms of coherent structures. While there may be other possibilities, these two scenarios are likely to be the most dominant events contributing to negative production. Control of coherent structures or their interactions via excitation can generate negative production in a flow which otherwise shows no negative production (see also Wygnanski, Oster & Fiedler 1979; Riley & Metcalfe 1980).

Non-zero production in the case of a single structure in a mixing layer requires that the cross-section of spanwise structures be non-circular and be inclined with the flow direction. For convenience, consider the simplistic case of an elliptic cross-section of the structure (figure 10). When the major axis of the ellipse is somewhat aligned with the direction of shear (configuration B in contrast with configuration A), the net coherent production is negative. Note that this is opposite to what one's intuition would suggest.

The second example is that of motions of two vortices around each other during the pairing process. Let us identify four successive phases of the pairing process by the configurations C, D, E and F (figure 11). Ideally, these four configurations can cyclically repeat themselves indefinitely. In reality, if the Reynolds number is high enough, merger typically takes place abruptly soon after the phase F. (In a low-Reynolds-number axisymmetric jet, the leapfrog motion of two adjacent vortex rings can continue for a few cycles before merger; see Reynolds & Bouchard 1981.) Detailed coherent Reynolds stress measurements show that the phase F produces significant counter-gradient Reynolds stress over the lower-speed half of the layer thickness.

Since either of these negative-production configurations (B and F in figures 10 and 11) is expected in general to occur randomly in space and time, their occurrence will not be strongly felt in a time average. However, if either can be made to occur successively at a fixed location, even the time average will show counter-gradient momentum transport by turbulence, hence negative production, at that location. Via appropriate excitation, we have been able to induce at fixed locations the stable pairing (i.e. pairing occurring repeatedly at a location) and configuration B of a single structure in plane and axisymmetric mixing layers. We have shown that this spatial localization produces time-mean negative production; see figure 3(*g*) for an example. The negative $\langle P \rangle$ data in figure 3(*f*) are lower than in figure 3(*g*) because the phase corresponding to figure 3(*f*) is different from that of configuration F, which dominates figure 3(*g*). In some flow situations, the excitation may be available naturally either via (settling chamber or other facility-related) resonance or via upstream feedback from structures themselves. This is what we suggest is happening in situations showing negative production.

4.3. *Production mechanisms: ribs*

From all the detailed measures of coherent structures in plane mixing layers and wakes, and circular and elliptic jets (discussed in §§3.2 and 3.5), we find that turbulence production is the maximum at the saddle, which is also characterized by

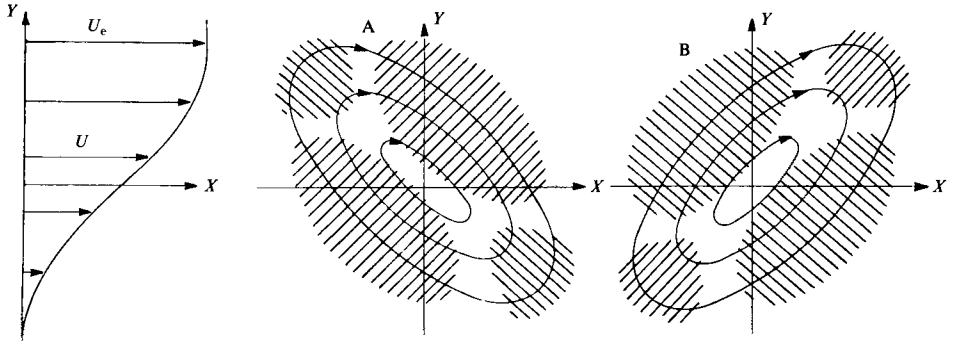

FIGURE 10. Negative production in a mixing layer due to a single structure; configuration A produces net co-gradient momentum transport and configuration B produces net counter-gradient momentum transport.

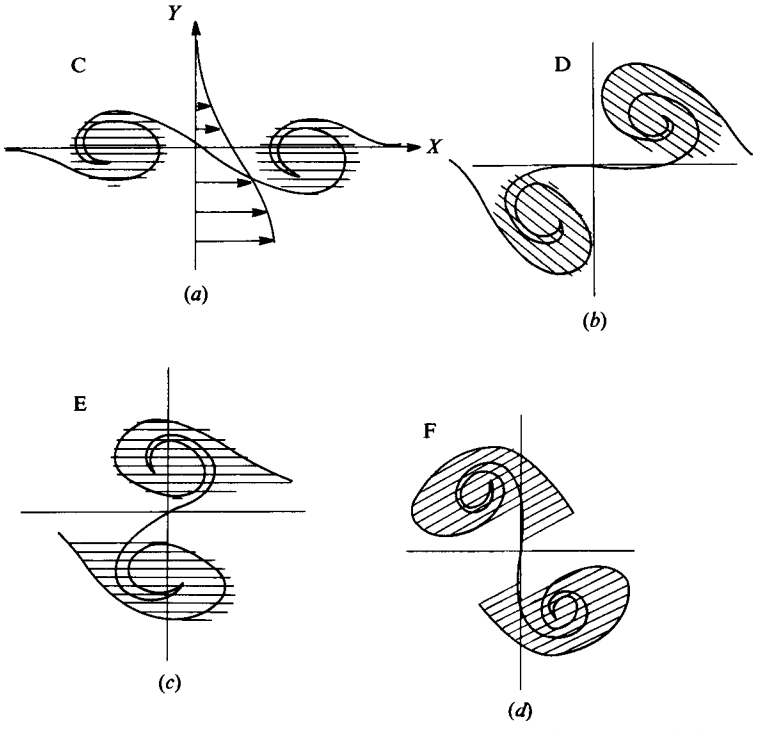

FIGURE 11. Schematics of four successive phases (configurations C, D, E and F) of the pairing process.

a very low value of spanwise vorticity. The relative configurations between coherent vorticity and production in these cases are the same as shown in figure 1(*b*). Since vortex stretching is the most likely mechanism for production, we concluded that the saddle (the so-called 'braid') region must consist of longitudinal vortices aligned with the diverging separatrix. Adjacent vortices in the 'braid' have opposite circulations so that the net circulation in the (y, z)-plane is zero. We have called these vortices 'ribs' (Hussain 1983*b*). The ribs have been visualized in a number of laboratories including ours (e.g. Bernal & Roshko 1986; J. Katz personal communication, 1983; C. R. Smith personal communication, 1983; Jimenez, Cogollos & Bernal 1985). Ribs

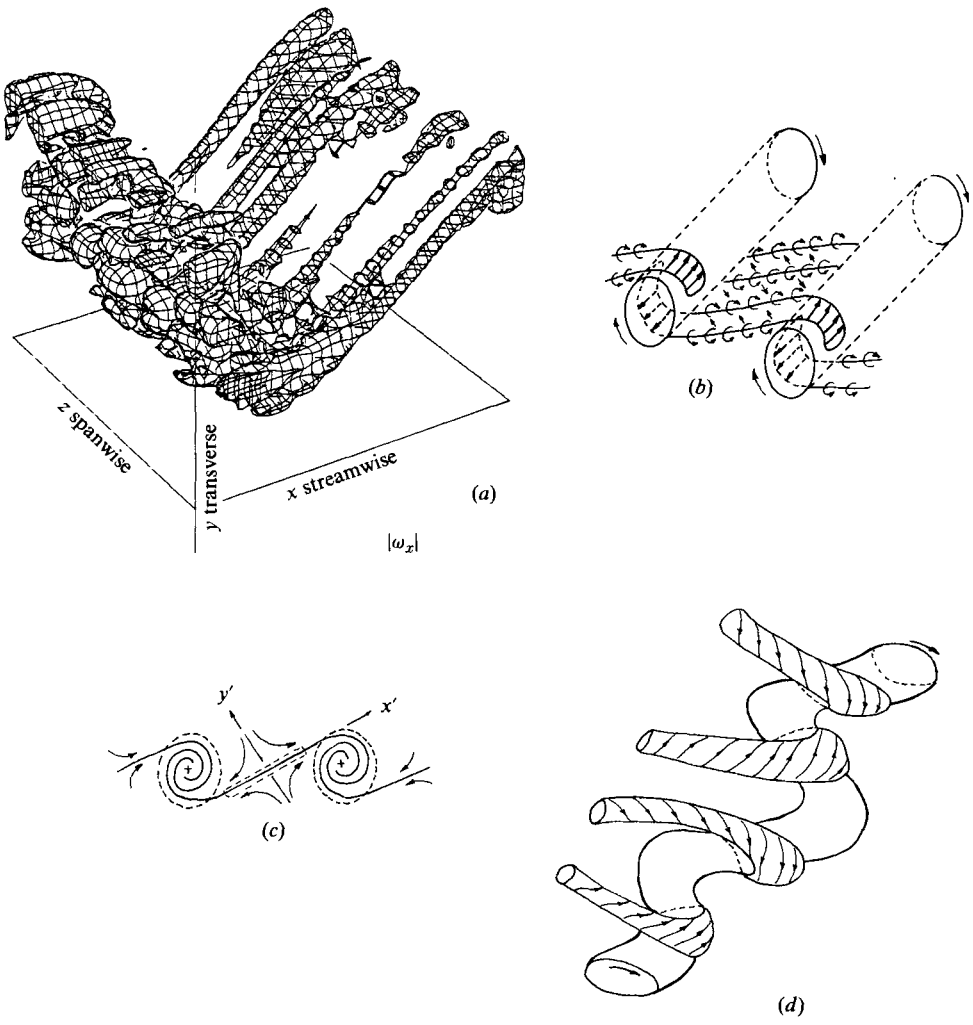

FIGURE 12. Dynamics of ribs: (*a*) direct numerical simulation; (*b*) schematic; (*c*) flow details around saddle; (*d*) a more realistic picture of ribs and rolls.

are clear in direct numerical simulations as shown in figure 12(*a*) (studied by us in collaboration with R. W. Metcalfe). The idealized schematic of the plane mixing layer and its end view are shown in figure 12(*b*, *c*), and a realistic schematic is shown in figure 12(*d*), where the spanwise contortions of the rolls induced by the ribs are also emphasized. Considering the plane wake as a combination of two opposed (and of course coupled) mixing layers lying on top of each other, the wake structure can be similarly interpreted.

Induced by these longitudinal vortical substructures, external fluid moves towards the turbulent shear flow region and can percolate through the braid region without being necessarily entrained. Thus irrotational external fluid approaching a mixing layer may escape entrainment. In the case of the wake, vortical fluid from one side of the wake can be entrained by structures on the opposite side.

The continual stretching of ribs causes them to spin faster due to conservation of angular momentum. This is equivalent to increasing velocity fluctuations and hence production of turbulence. In reality, the stretching enables the ribs to counter the

decay due to viscous diffusion and retain their spin. Viscous diffusion transfers vorticity to the ambient non-vortical fluid that is drawn towards the shear flow. Thus the underlying mechanism for production and entrainment is the same, namely vortex stretching. As a result of stretching by the primary structures, spinning turbulent fluid is advected away from the saddle, where new turbulence (i.e. spinning) is continually produced. However, the location of production is not that of mixing, as the spin is aligned with the diverging separatrix; mixing must mean acquisition of three-dimensional, random vorticity. When this entrained fluid at the saddle with (one-dimensional) vorticity aligned with the diverging separatrix reaches the primary structure fluid with large-scale spanwise vorticity, the interaction of the two orthogonal vorticities produces three-dimensional turbulence and mixing. Thus the connection point of the ribs with the rolls is the site of most true mixing. As the ribs are wrapped around the rolls, vortex lines are turned and aligned with the coherent flow, thus causing large contributions to coherent helicity (see §4.4). The action of the rolls is to take this turbulent fluid and deposit it in the structure core. This is the mechanism for continual replenishment of structure turbulence, which would otherwise decay due to dissipation. Thus one can say that coherent structures have a built-in mechanism for their own survival, albeit short-time survival. Based on these observations, we claimed that 'vortex stretching is the physical mechanism for entrainment and production in all turbulent flows' (Hussain 1983*b*).

The physics of the mixing layer, and perhaps of all shear flows, as unfolded above, is rather at variance with the accepted notions in turbulence. Since vortex stretching appears to be the key mechanism for production, the rapid distortion theory (Batchelor & Proudman 1954; Hunt 1973, 1985) seems to be more appropriate here than shear production suggested in standard texts. Since mixing, hence dissipation, occurs at the connection points of ribs with rolls, the sites for dominant production and dissipation seem to be different. The prevalent notion is that turbulence is first produced in u and then transferred to v and w by the isotropizing role of pressure (Tennekes & Lumley 1974). However, since the diverging separatrix is nearly in the streamwise direction, turbulence is produced first primarily in v and w components, which then contribute to u as the ribs wrap around the rolls; of course, since ribs are inclined with x, one can say that turbulence is produced simultaneously in u, v and w components. Even though these discussions address the plane mixing layer, these points equally apply to other flows.

4.4. *Helicity and dissipation*

There has been some interest in coherent structures in connection with turbulent flow topology. A key feature of this topology is helicity and its connection with coherent structures. Moffatt (1969) introduced the concept of helicity,

$$H = \int \boldsymbol{u}\cdot\boldsymbol{\omega}\,\mathrm{d}V = \int h\,\mathrm{d}V,$$

and showed that, when integrated over the entire flow domain, H is an invariant of the Euler flow. This global invariant, however, says nothing about local values of helicity density $h = (\boldsymbol{u}\cdot\boldsymbol{\omega})$, which can (and presumably must) have large spatial variations, especially because turbulent flow is far from equilibrium (Levich, Levich & Tsinober 1983). Hereinafter, helicity is loosely used to denote helicity density. For a vortex element not completely orthogonal to the local velocity, the local helicity is non-zero. Now, wherever $\boldsymbol{u}\cdot\boldsymbol{\omega}$ is large, the vector quantity $\boldsymbol{u}\wedge\boldsymbol{\omega}$ is small because of the trigonometric identity,

$$|\boldsymbol{u}\cdot\boldsymbol{\omega}|^2 + |\boldsymbol{u}\wedge\boldsymbol{\omega}|^2 = |\boldsymbol{u}|^2|\boldsymbol{\omega}|^2.$$

Note that in the Navier–Stokes equation,

$$\frac{\partial \boldsymbol{u}}{\partial t} + \boldsymbol{u} \wedge \boldsymbol{\omega} = -\nabla\left(\frac{p}{\rho} + \frac{u^2}{2}\right) + \nu\nabla^2\boldsymbol{u},$$

the nonlinear term $\boldsymbol{u} \wedge \boldsymbol{\omega}$ is responsible for cascade from larger to smaller scales – the mechanism by which larger scales decay. Also, in the case of reduced cascade, there will be reduced production of fine scales and hence reduced dissipation. Since $\boldsymbol{u} \wedge \boldsymbol{\omega}$ is analogous to the Coriolis force, $\boldsymbol{u} \wedge \boldsymbol{\omega}$ can also be viewed as a vortex force locally moving a vortex filament transverse to it (in a direction normal to the plane defined by $\boldsymbol{u}$ and $\boldsymbol{\omega}$). Thus $\boldsymbol{u} \wedge \boldsymbol{\omega}$ contributes to the local kinking of vortex filaments, and thus to vortex stretching; it is related to turbulent momentum transport in a turbulent flow.

It therefore follows that helical structures will have low dissipation and can therefore be expected to be long-lived. Levich *et al.* (1983) and Moffatt (1983) suggested that coherent structures are helical. [This suggestion has to be limited to three-dimensional structures as helicity is identically equal to zero for toriodal structures in the near field of an axisymmetric jet or the Brown–Roshko rollers of the plane mixing layer. On the other hand, three-dimensionality of structures implies non-zero helicity. Thus the claim that three-dimensional coherent structures are helical (Tsinober & Levich 1983) is not surprising. Also, this suggestion is inconsistent with our observation of the structure life time (§2.5.4)] It follows from the above reasoning that most dissipation must occur outside coherent structures; that is, domains of large helicity and dissipation are spatially exclusive. Moffatt (1985) showed as a consequence of flow topology that regions of large helicity must be separated by sheets of dissipation. While Moffatt's ideas are relevant to Euler flows where vortex dynamics and interactions are intrinsically different from those in a Navier–Stokes flow, there is some basis for assuming that these ideas are relevant to coherent structures because (large-scale) coherent structure dynamics is essentially inviscid. Even though dissipation peaks may occur outside helical structures, it is not likely that the total dissipation is dominated by these peaks. Obviously there is dissipation within the coherent structures, which can be significant.

Direct measurement of instantaneous vorticity in turbulent flow is virtually an impossible task. Wallace (1986) and Frish & Webb (1981) seem to be the only ones who have successfully measured it. A realistic probe for local measurement of vorticity is not yet available. Thus measurement of helicity is extremely difficult. The measurement of dissipation is equally difficult; some estimates can be made on the assumptions of local isotropy and Taylor hypothesis (for example, Antonia, Satyaprakash & Hussain 1982). We have taken advantage of direct numerical simulation of turbulent flows to compute helicity and dissipation contours in a mixing layer (this research is being done in collaboration with R. W. Metcalfe). Figure 13 (*a–c*) shows the contours of spanwise vorticity, helicity and dissipation in the streamwise-transverse (x, y)-plane. The spanwise vorticity ω is shown in order to indicate the relative location of coherent structure in the mixing layer. The dominant contours of helicity and dissipation in figure 13 (*b*, *c*) have been superposed in 13 (*d*). Note that helicity contours consist of positive and negative values. It is apparent that while there are overlapping domains of helicity and dissipation contours, their peak regions do not overlap, lending some support for the spatial exclusiveness of domains of dissipation and helicity. One must recognize that this flow is still in a transitional stage, and a test of the conjecture about spatial exclusiveness of helicity and dissipation is yet to be made in a more turbulent stage of the flow. Numerical simulations by Pelz *et al.* (1985, 1986) suggest that in turbulent flows velocity and

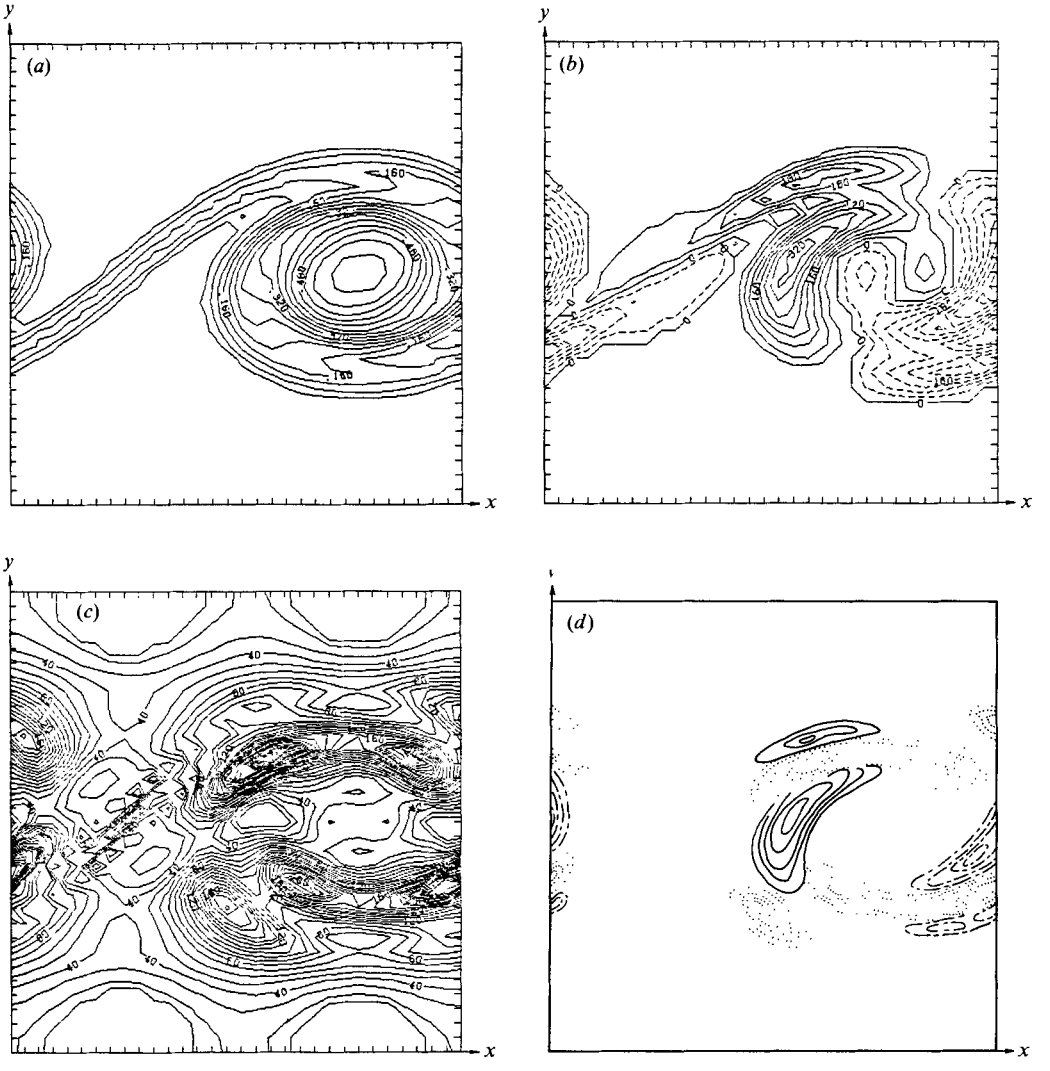

FIGURE 13. Plane mixing layer structure topology from direct numerical simulation. Contours in the (x, y)-plane of: (*a*) spanwise vorticity; (*b*) helicity with positive (solid lines) and negative (dashed lines) values; (*c*) dissipation; (*d*) comparisons of helicity (solid and chain-link lines) and dissipation (dotted lines) contours; contours in (*d*) highlight peak regions of (*b*) and (*c*). Contour values in (*a*)–(*d*) are not indicated, as relative locations of contour peaks only are of interest here.

vorticity tend to be aligned; the results of Kerr & Gibson (1985) are somewhat different, presumably because of forcing and the different spectrum used initially in this case (Levich and Shtilman personal communications).

Two points need to be emphasized. First, by definition, $\boldsymbol{u}\cdot\boldsymbol{\omega}$ is not Galilean invariant. This obvious point seems to have escaped emphasis until noted by Speziale (personal communication, 1985). It seems to me that a logical choice would be to take $\boldsymbol{u}\cdot\boldsymbol{\omega}$ in a frame advected with the structure centre. Secondly, since helicity can have large fluctuations with a variety of scales, most helicity within a structure will be phase incoherent. Thus, one needs to define both coherent and incoherent helicities, i.e. $-\langle\boldsymbol{u}\rangle\cdot\langle\boldsymbol{\omega}\rangle$ and $-\langle\boldsymbol{u}_{\mathrm{r}}\cdot\boldsymbol{\omega}_{\mathrm{r}}\rangle$, where the brackets indicate phase average. Coherent helicity is meaningful only when eduction is performed after careful alignment as outlined in §3.5.

4.5. *Coherent structures and aerodynamic noise*

A primary example of the use of the coherent structures approach is aerodynamic noise. Although there is a general consensus that coherent structures are important in aerodynamic noise generation, neither the generation mechanism nor the significance in jet noise is known yet. Laufer (1974) proposed that pairing was the principal mechanism for jet-noise generation. However, we immediately contended that this mechanism was very unlikely. For an initially laminar jet, most of the pairing activity occurs in the shear layer mode near the lip of the jet and is complete within about one diameter from the jet exit, while most noise originates from near the end of the potential core, say, between 4 to 8 diameters (Juvé, Sunyach & Comte-Bellot 1980). In this early region, shear-layer pairing can produce significant sound; but most jet noise is produced near the end of the potential core. Moreover, most practical jets, being turbulent at the exit, seldom involve pairing of vortices. The initially turbulent mixing layer rolls up, typically at the jet column mode, thus bypassing the shear-layer mode. These facts suggest that pairing – whether induced or occurring naturally – even though capable of producing sound, cannot be the dominant cause of noise in practical jets.

Our proposition is that it is the breakdown process of the initial toroidal structures into substructures near the end of the potential core and their interactions that produce most noise (Hussain & Zaman 1981; Hussain 1980, 1983*a*). It is quite likely that the breakdown process involves the cut-and-connect mechanism by which substructures result from the initial toroidal structure (see figure 14). We believe that this mechanism is also responsible for the avalanche of three-dimensional and smaller-scale motions, mixing, and generation of high turbulence and Reynolds stress at the end of the potential core. This mechanism may be central also to the generation of enstrophy and helicity in turbulent flows (Levich, personal communication).

4.6. *Cut-and-connect mechanism of vortex interaction*

A turbulent flow can be viewed as a tangle of vortex filaments. Even in transitional flows, initially rolled-up two-dimensional vortical structures develop three-dimensionality through secondary instability and then undergo interactions. A study of vortex interactions is obviously crucial to understanding transition processes as well as basic turbulence phenomena such as transport, mixing, turbulence production, and generation of aerodynamic noise. A highly interesting aspect of vortex interactions is the cut-and-connect process during which two adjoining vortex filaments are cut and connected after switching, i.e. they are cross-linked. This curious phenomenon (topological transformation) has been observed experimentally by a number of investigators (Hama 1960; Crow 1970; Kambe & Takao 1971; Oshima & Asaka 1977) but has so far remained unexplained. Theoretical analysis is obviously complicated because of the intricate three-dimensional nature of the process and because the event occurs rapidly and must involve viscosity, as such a process is impossible without viscosity. The cut-and-connect provides an alternative mechanism for energy cascade and a mechanism for generation of helicity (and thus perhaps coherent structures). We have analysed an idealized model utilizing the vorticity equation and geometrical symmetries, and applied this analysis to the prediction of turbulent jet noise. The analysis involves superposing a small vortex ring at the interaction region so that the vorticity of the ring cancels that of the filaments and also makes the connections as shown in figure 15(*a*). We invoke the conservation of impulse $\boldsymbol{P} = (\frac{1}{2})\rho \int \boldsymbol{r} \wedge \boldsymbol{\omega}\, dv$ during the interaction; ρ is the fluid density, $\boldsymbol{r}$ is the

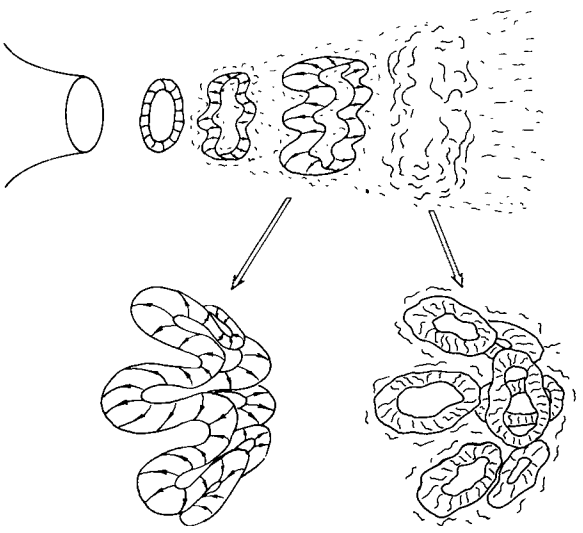

FIGURE 14. Idealization of the breakdown process in the circular jet.

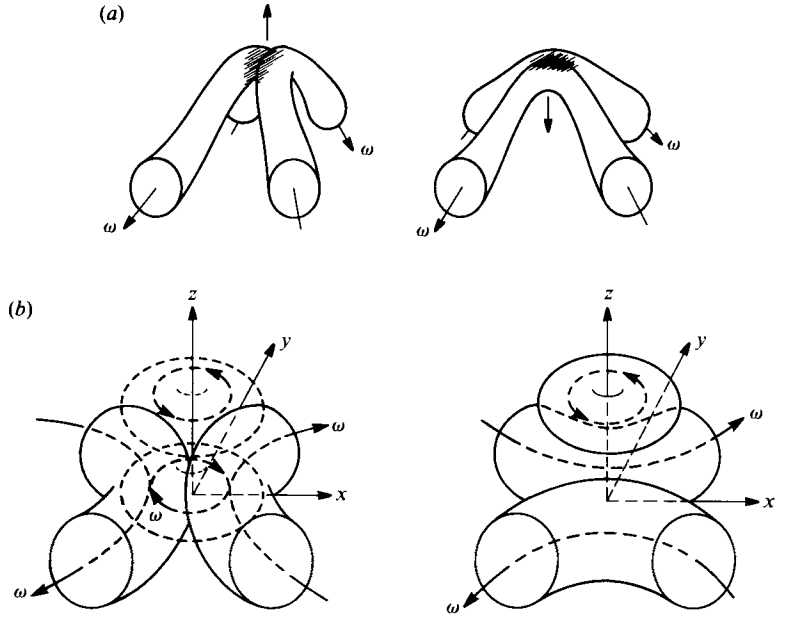

FIGURE 15. (*a*) Vortex configurations before and after the cut-and-connect process; (*b*) assumed mechanism of the recoil vortex.

position vector, $\boldsymbol{\omega}$ is the vorticity, and the integration is taken over the interaction volume. Since the superposed vortex has downward impulse we need to further superpose a *recoil* motion with upward-directed impulse. Hence the recoil vortex ring shown in figure 15(*b*).

The fluid motion is analysed by invoking the geometric symmetry conditions on the initial and final states and by expanding the velocity $\boldsymbol{u}$ and vorticity $\boldsymbol{\omega}$ fields in these two states as polynomials of coordinates. As shown in figure 15(*b*), the two

filaments have two planes of inversion symmetry, namely the (x, z)- and (y, z)-planes, and the recoil vortex has an axisymmetry about the z-axis. The coefficients of the polynomial are determined from the two states and the complete three-dimensional vorticity equation. The resulting solution is in terms of a single function $T(t)$,

$$\frac{\mathrm{d}T}{\mathrm{d}t}+\frac{T(T-1)}{t^*}=0 \quad \text{where } t^*=O\left(\frac{\Gamma}{\sigma^2}\right).$$

Here, Γ is the circulation and σ is the vortex core radius. The solution $T=e^\tau/(1+e^\tau)$, where $\tau=t/t^*$, has the expected behaviour as it varies from 0 to 1 in a very short time $O(t^*)$. The velocity and vorticity fields through the process can be expressed in terms of T but are too detailed to discuss here (a forthcoming paper by Takaki & Hussain will give details).

4.6.1. *Prediction of jet noise*

The far-field sound pressure caused by a cut-and-connect event can be estimated from Lighthill's (1952) formula for a compact source. The jet noise can be estimated by assuming that cut-and-connect events occur around initial vortex rings in the jet near field because of lobe formation due to the Widnall instability. The effect of the jet mean flow is considered by applying Goldstein's (1984) formula. For a realistic inclination of the interacting vortex filament, the sound intensity I is estimated as (see Takaki & Hussain 1985, for details),

$$I\approx\left(\frac{\rho D\sigma}{a^5r^2}\right)\left(\frac{d}{\sigma}\right)^6U^8.$$

Here D is the jet diameter, d is the mean vortex spacing, a is the ambient acoustic speed, and U is the jet velocity. This formula shows qualitative agreement with experimental data of Lush (1971). The U^8 dependence is consistent with Lighthill's prediction for quadrupole sources. The factor $(d/\sigma)^6$ is a new result emphasizing the critical importance of the degree of vorticity concentration.

4.6.2. *Pairing and vortex sound*

We feel that the role in aerodynamic noise of coherent structures – whether pairing or not – can be better explained in terms of vorticity dynamics. The relationship between vorticity and far-field pressure was first proposed by Powell (1964) in the form of an acoustic analogy. His vortex sound theory has subsequently received further simplifications and interpretations by Howe (1975), Mohring (1978) and Obermeier (1985). Powell was able to show that the source term was $\nabla\cdot\boldsymbol{\omega}\wedge\boldsymbol{u}$ ($\boldsymbol{\omega}$ being vorticity and $\boldsymbol{u}$ the velocity); this contrasted the Reynolds stress and dilatation representations of Lighthill (1952) and Ribner (1962), respectively. Mohring showed that the far-field pressure of a jet could be expressed in a form linear in vorticity, thus allowing superposition of all vortical sources in the tensor term $\boldsymbol{Q}=\partial^3/\partial t^3\int_{\mathrm{V}}\boldsymbol{y}(\boldsymbol{y}\wedge\boldsymbol{\omega})\,\mathrm{d}^3\boldsymbol{y}$, which is the heart of his formulation. Here V denotes the compact domain of the vortical fluid. This expression clearly emphasizes how time variation of vorticity can contribute to sound. For a vortical structure to contribute to sound, it must contribute to $\boldsymbol{Q}$. Even though speculations abounded about the role of pairing in aerodynamic noise generation (Ffowcs-Williams & Kempton 1978; Kibens 1980; Crighton 1981; Zaman 1985), precisely how pairing can produce sound was never addressed until recently by Bridges & Hussain (1986). When a jet is initially turbulent, vorticity at the scale of the structures is diffuse; thus time variations of both $\boldsymbol{y}$ and $\boldsymbol{\omega}$ will be weakened and $\boldsymbol{Q}$ will be decreased.

Since so much of coherent structure dynamics has been discussed in terms of pairing, perhaps it is worth asking: What is pairing? It is meant to be a flow event when two vortical fluid lumps merge to form a single vortical lump. In fact, the entrapment of ambient fluid between two (or more) merging vortical lumps was proposed as the primary mechanism of entrainment (Winant & Browand 1974), even though Hernan & Jimenez (1982) found by image processing of the mixing layer films of Brown & Roshko (1974) that 80 % of entrainment involved no pairing. The concept of pairing appears elusive, especially for aerodynamic noise generation. In a turbulent shear flow, vortical structures are influenced by other structures via Biot–Savart induction; they can begin interacting before they come into physical contact. In early regions of jets and shear layers such induction leads to merger. However, pairing-like motions need not result in actual merger/pairing. Acceleration of vorticity-bearing fluid elements – pairing or not – can occur in a turbulent or unsteady flow, contributing to Q and thus to far-field noise.

5. Studies of technological relevance

We have carried out a number of studies with the objective of modifying (both enhancing and suppressing) turbulence through manipulation of coherent structures and their interactions. Such manipulation has been effected by passive (e.g. geometry modification) or active (e.g. excitation) means, involving intricate couplings of various instability and feedback modes, and has important technological applications (Roshko & Reynolds, personal communication). In the following, we will review some of our results pertaining to response of jets to excitations. Understanding of these basic aspects is crucial to achieving turbulence management.

5.1. *Preferred mode and effects of excitation of circular jet*

The circular jet evolving from a contraction nozzle has two lengthscales: the exit boundary-layer thickness (say, the momentum thickness θ_e) and the jet diameter D. Associated with these two scales there are two distinct modes of instability as well as two distinct modes of structure interaction such as pairing. These two instability modes were investigated by Zaman & Hussain (1977) and were characterized by them as 'shear layer mode' and 'jet column mode'. Sufficiently close to the nozzle and with a top-hat exit flow profile (i.e. $\theta_e/D \ll 1$), the mixing layer of the circular jet is not dissimilar from that of the extensively investigated plane layer. This is true for $x \lesssim \frac{1}{2}D$ for which θ_e (or alternatively the instability wavelength λ) is the appropriate lengthscale. Further downstream, say at $x \approx D$, the mixing-layer thickness becomes comparable to D, and thus the effect of the azimuthal curvature can no longer be ignored. In this region, D is the appropriate lengthscale. Since θ_e and D can be fairly arbitrarily varied, shear-layer phenomena and jet-column phenomena should be expressed in terms of θ_e and D as the corresponding lengthscales, respectively. The incorrect use of D as the lengthscale characterizing near-field jet behaviour is still frequent.

The initially laminar shear layer has been found to roll up at $St_{\theta_e} = 0.012$ (Zaman & Hussain 1977, 1980), while the theoretical value is $St_{\theta_e} \approx 0.017$ (Michalke 1965; Freymuth 1966). This apparent contradiction can perhaps be reconciled by the fact that $St_{\theta_e} \approx 0.012$ corresponds to the case of maximum amplification while $St_{\theta_e} \approx 0.017$ corresponds to the case of maximum amplification rate. That is, when excited at one frequency at a time, $St_{\theta_e} \approx 0.012$ produces the largest disturbance amplitude, but $St_{\theta_e} \approx 0.017$ produces the largest growth rate (obviously with a larger

λ in the former case). The fact that natural (i.e. unexcited) instability occurs at $St_{\theta_e} \approx 0.012$ appears to be clear evidence of feedback. The occurrence of feedback has been debated at length but remains unsettled. The induced velocity at the lip due to two rolled-up vortices 1 and 2 at two St_{θ_e} values (i.e. 0.017 and 0.012) will be Cu_1 and Cu_2, where C is a constant, and u_1 and u_2 are the saturation disturbance velocities associated with $St_{\theta_e} = 0.017$ and 0.012, respectively. Because $u_2 > u_1$ and ambient disturbances in an unexcited flow occur in a broadband range of frequencies, $St_{\theta_e} \approx 0.012$ will experience the strongest feedback at the lip and will be sustained by feedback. That is, given a broadband range of ambient disturbances, the disturbance at $St_{\theta_e} \approx 0.012$ will dominate.

Further downstream, i.e. near the end of the potential core, the instability scales on the jet diameter, D. The corresponding value of St_D characterizes the jet preferred mode. Based on excitation data for $St_D \leqslant 0.6$, Crow & Champagne (1971) suggested that the preferred mode was that which produced the maximum amplification of the centreline total turbulence level u_t'. They found that the growth rate of u_t' increased with increasing St_D until $St_D = 0.3$ and then dropped; they thus identified $St_D \approx 0.3$ as the preferred mode. Extending the St_D range to higher values, Zaman & Hussain (1977, 1980) found that $St_D \approx 0.85$ produced the highest u_t', even higher than that at $St_D = 0.3$. They redefined the jet preferred mode to be that frequency at which the *fundamental* amplitude u_f' receives the maximum amplification. This is a non-trivial point since u_t' can differ considerably from u_f'.

Why does the preferred mode St_D value reported in the literature vary over a range? A number of factors can cause the discrepancies. First, the frequency of the peak in the time-averaged spectrum varies considerably in x and r. This variation has three origins: (i) because of pairing, average frequency can drop with increasing x (Browand & Laufer 1975); (ii) there can be a large radial variation of structure passage frequency (as much as threefold) as shown by Lau & Fisher (1975) and others, which has been attributed to partial and fractional pairings by Hussain & Clark (1981); (iii) the tilting of non-circular structures as they are advected downstream is an additional source of radial variation of structure passage frequency (Hussain & Zaman 1981). Thus, for reference and comparison purposes, the measurement location for identifying the preferred mode must be precisely stated. For jets with top-hat exit profile, the end of the 'time-mean' potential core on the jet centreline, say, $x/D = 4$, is a good reference point. Secondly, the identification of the preferred mode from spectra in an unexcited jet is typically not meaningful, as jets are almost always 'driven' because of various unavoidable tunnel acoustic modes and ambient disturbances (typically laboratory acoustic modes) which manifest as free-stream turbulence (Hussain 1980). If these disturbances fall within the receptivity band of the jet or shear layer (M. Morkovin, personal communication), these will be amplified (at a rate depending on the disturbance frequency and amplitude). Thirdly, as already mentioned, determination of the preferred mode should be based on u_f' and not on u_t'. The excitation amplitude should be small but sufficiently above the background disturbance or 'free stream turbulence' level. Most studies of the preferred mode have paid little attention to these details.

It is worth mentioning here that because of the background (mostly acoustic) disturbance modes, which do not vary (at least not continuously) with U_e, many researchers have reported steps in the f *vs.* $U_e^{\frac{3}{2}}$ relation for shear layer or jet instability frequency f. We think that these steps are spurious and must be due to lock-in of the shear-layer instability to various acoustic modes of the tunnel or laboratory environment. This controversy can be conclusively settled by determin-

ing, via controlled excitation of jets over a range of frequencies and diameters, the frequency f_m which produces the maximum disturbance growth rate at each U_e. In the resulting f_m *vs.* $U_e^{\frac{3}{2}}$ plot such steps should disappear.

5.2. *Excited elliptic jet*

The distinctly different responses to excitation of circular and plane jets suggested to us interesting technological possibilities for jets of other geometries. Being motivated by the fact that the elliptic configuration is more general than circular and plane jets, we have studied excited and unexcited elliptic jets (along with other irregular shapes). Because of the effect of azimuthal curvature on self-induction (Batchelor 1967 p. 510), hence advection, of different parts of an elliptic vortex loop, we expected the evolution of large-scale coherent structures (and their modification by controlled excitation) as well as mixing phenomena in the near field of an elliptic jet to be quite different from that of a circular jet. With this in mind incompressible elliptic jets of moderate aspect ratios have been studied experimentally employing both hot wires and flow-visualization methods (Husain 1984).

The experiments were carried out using nozzles of aspect ratios 2:1 and 4:1, both having the same exit area at the Reynolds number $Re_{D_e}(\equiv U_e D_e/\nu) = 10^5$. Here $D_e(=2(ab)^{\frac{1}{2}}$, where a and b are the semiaxes of the elliptic cross-section at the exit plane) is the equivalent diameter (5.08 cm) of the elliptic cross-section at nozzle exit (contraction ratio 25:1). In order to focus on the effect of the elliptic geometry alone, the spanwise variation of the exit boundary layer was eliminated. The coherent structures and their interactions in the elliptic jet near field are found to be characterized by 'preferred' and 'stable pairing' modes as in circular jets, and they scale on D_e. The corresponding values of the Strouhal number based on D_e are also the same as in circular jets. However, the pairing process in elliptic jets is somewhat different from that in a circular jet. Elliptic large-scale vortical structures are found to pair along a short segment in the initial major axis side, while in the initial minor axis side the trailing vortex, instead of pairing, rushes through the leading vortex and then abruptly breaks down. The large intensity u_t' is then the induced 'footprint' of the partial vortex pairing events.

Because of curvature-dependent self-advection of vortex filaments (Batchelor 1967), elliptic vortex rings switch axes. This is also the reason why the cross-section of elliptic jets switch axes. The spreading of elliptic jets is quite different from that of circular and plane jets. The locations for switchover of elliptic cross-section can be drastically altered by controlled excitation, depending on the Strouhal number. The equivalent diameter $D_e(x)$ of an excited elliptic jet is greater than that of an excited circular jet. This increase in the spreading of an elliptic jet is highly pronounced under strong forcing at the preferred mode, i.e. at $St_{D_e} \approx 0.4$. For excitation at the preferred mode, the local jet half-width B along the major and minor axes are shown in figure 16 (a, b) for 2:1 and 4:1 elliptic jets. Up to $x/D_e = 20$, major and minor axes switch twice (when excited) in the 2:1 jet but once in the 4:1 jet. Also, excitation moves the switchover location upstream. Note that for $x/D_e > 5$, the elliptic cross-section is rotated by 90° between the two jets. The jet spread data for 2:1 and 4:1 elliptic jets suggest that as the aspect ratio of the nozzle increases, the spreading along the minor axis becomes more dominant. [Flow visualization in our laboratory has revealed that elliptic vortex rings in an excited elliptic jet can bifurcate into two rings, thus producing enhanced mixing.] Both jets showed maximum increase in cross-sectional area (due to excitation) near the location where turbulence intensity was maximum; these area increases for the 2:1 and 4:1 jets were

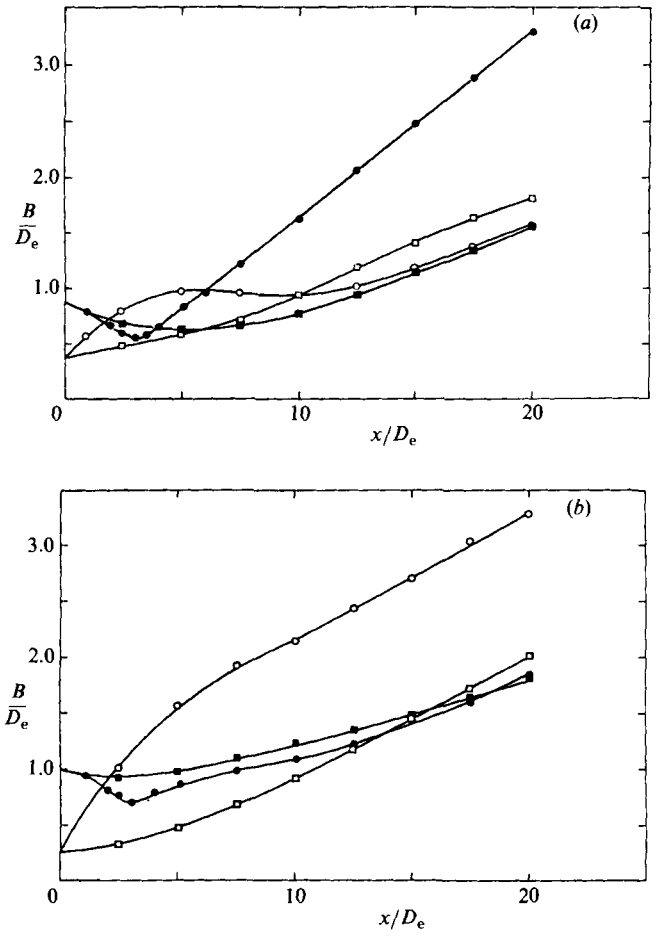

FIGURE 16. Width of excited ($St_{\theta e} = 0.4$, $u_c'/U_e = 0.15$) and unexcited elliptic jet. (*a*) 2:1 elliptic jet; (*b*) 4:1 elliptic jet. The equivalent diameter $D_e = 5.08$ cm; $U_e = 30$ m/s; $Re_{D_e}(\equiv U_e D_e/\nu) = 10^5$. In the initial major axis plane: ●, excited; ■, unexcited. In the initial minor axis plane: ○, excited; □, unexcited.

150% and 190%, respectively (figure 17). This maximum increase in the jet cross-sectional area at the station where the jet is well mixed and turbulence intensity is also the maximum confirms the role of excitation in enhancing mixing. This enhancement is considerably more than that produced by corresponding excitation of a circular jet (also shown in figure 17), even more than that produced by self-sustained forcing with a whistler nozzle (see §5.4), thus suggesting interesting technological possibilities for excited elliptic jets. Some of these are under investigation in our laboratory.

5.3. *Turbulence and noise suppression using excitation*

While controlled excitation typically organizes and enhances instability, experimentations revealed turbulence suppression (by as much as 80%) near the exit of an axisymmetric jet under controlled excitation (Zaman & Hussain 1981). We found our data puzzling because Crow & Champagne's (1971) data showed no such suppression; it now appears that it is not likely that suppression could be avoided.

Explorations in a number of axisymmetric and plane jets and plane mixing layers

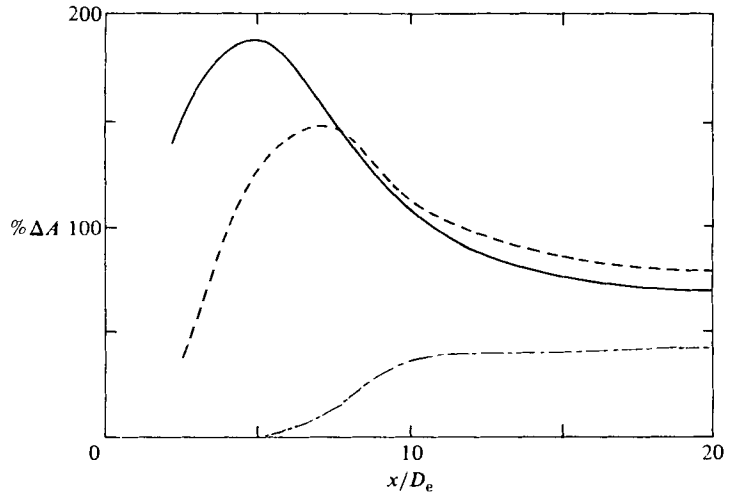

FIGURE 17. Percentage increase in jet cross-sectional area of circular and elliptic jets under excitation ($u'_e/U_e = 0.15$) at the preferred mode. Jet flow state is same as in figure 16. – – – –, 2:1 elliptic jet; ———, 4:1 elliptic jet; —·—, circular jet.

in our laboratory helped us to establish the universal nature of this suppression phenomenon and its unique connection with the shear-layer structures (Zaman & Hussain 1981). In circular jets, the suppression occurs over the range $0.75 < x/D < 8$, while in the plane mixing layer suppression can be detected as far as $x/\theta_e \approx 6000$. The suppression effect produced by controlled excitation is summarized in figure 18(*a*, *b*) by plotting the ratio of longitudinal peak fluctuation intensity under excitation (u'_{ex}) to the unexcited value (u'_{ux}). Figure 18(*a*) shows that the suppression is the maximum at the Strouhal number $St_{\theta_e} \approx 0.017$; at a given frequency f_p of excitation, St_{θ_e} variation was achieved by changing the jet speed. Figure 18(*b*) shows that u'_{ex}/u'_{ux}, measured along a y = constant line in a number of facilities, becomes minimum at $x/\theta_e \approx 400$. Note that other components of turbulence and the Reynolds stress also show similar reductions due to excitation (Zaman & Hussain 1981). It was shown that suppression is a straightforward consequence of earlier breakdown, induced by the excitation, of the shear-layer vortices which otherwise naturally grow to larger sizes and survive for larger x. Excitation at $St_{\theta_e} \approx 0.017$ produces a growth of the instability wave considerably higher than the natural instability (occurring at a lower St_{θ_e}) and thus produces earlier saturation, roll-up, breakdown, and an associated inhibition of pairing. The result is a reduction everywhere of fluctuation intensities and the Reynolds stress. The suppression discussed here is different from the excitation-induced suppression (tail-pipe effect) in a jet resulting from the superposition of acoustic and hydrodynamic waves (Rockwell & Schachenmann 1982). A possible coupling of these two separate effects is interesting and needs to be investigated. The turbulence suppression effect has been investigated numerically by representing the shear layer by an array of a large number of point vortices, and the sensitivity of the suppression effect to the excitation frequency and amplitude has been verified (Nallasamy & Hussain 1984).

Our speculation that the turbulence suppression by controlled excitation would probably also cause noise suppression (Zaman & Hussain 1981) was verified by noise measurements of excited subsonic jets in a large, quality anechoic chamber. The jets were excited in the shear-layer mode by injecting sound through a thin slit along the

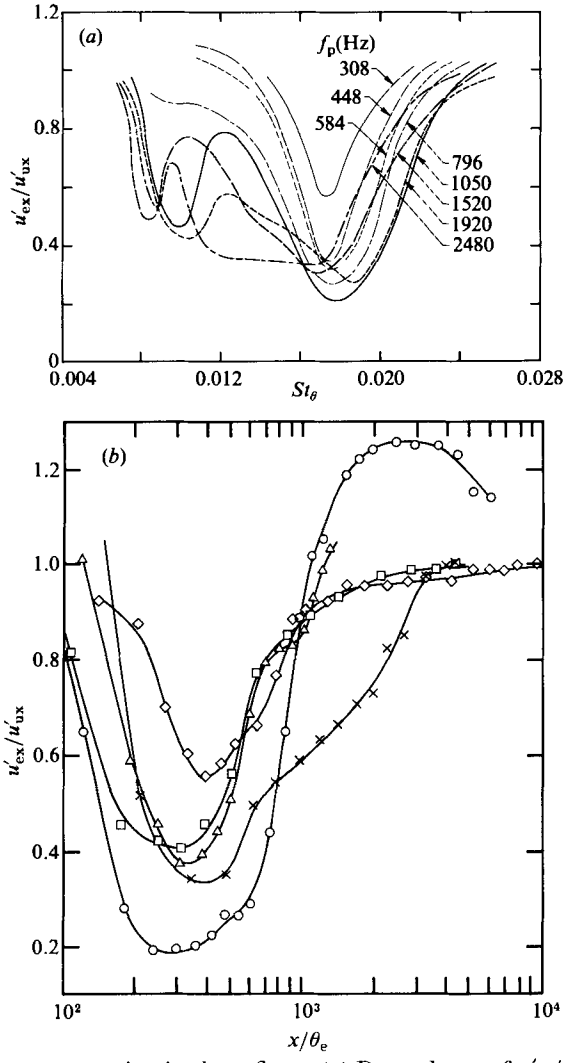

FIGURE 18. Turbulence suppression in shear flows. (*a*) Dependence of u'_{ex}/u'_{ux} on St_{θ_e} measured on the centreline of a 2.54 cm jet at $x/D = 4$ for different f_p; (*b*) downstream variation of u'_{ex}/u'_{ux} for $St_\theta = 0.017$, measured along a y = constant line near the lip. ×, 18 cm circular jet; ○, 2.54 cm circular jet; △, 3.18 cm plane jet; □, single-stream mixing layer at $U_e = 10$ m/s; ◇, single-stream mixing layer at $U_e = 20$ m/s.

lip. Far-field measurements revealed that the noise suppression due to excitation was broadband. When the spectral peak at the excitation frequency is removed from the spectrum, the OASPL resulting from the integration of the area under the spectrum then gives a measure of the modification of the sound field. Figure 19 shows that noise 's suppressed by excitation in the St_{θ_e} range of 0.01–0.02. Hot-wire measurements in the same facility revealed a broadband turbulence suppression associated with the noise suppression; the spectral range for turbulence suppression agrees with that for noise suppression. The far-field sound spectrum is devoid of any sharp peaks at subharmonics; thus this broadband suppression is not due to organization of pairing (Kibens 1980). It is especially interesting to note that the excitation-induced noise suppression is a net suppression even when the excitation sound is included. Further details have been recorded by Hasan (1983).

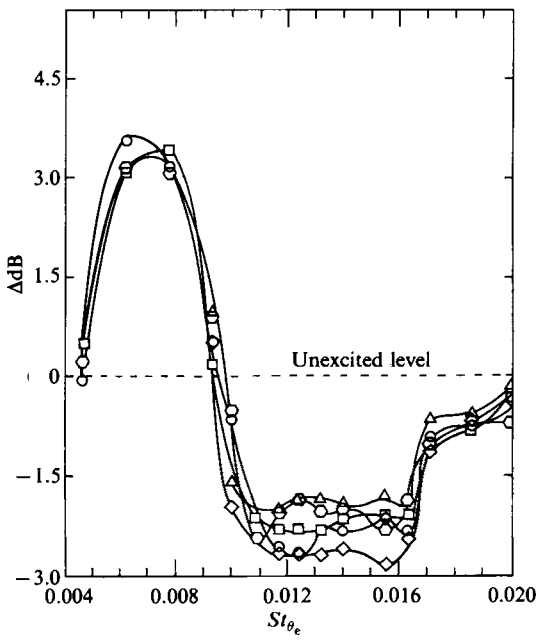

FIGURE 19. Aerodynamic noise suppression for an excited circular jet (4 cm diameter) at Mach number = 0.15 as a function of St_{θ_e}. Data are for different emission angles ϕ. □, $\phi = 45°$; ○, $\phi = 60°$; △, $\phi = 75°$; ○, $\phi = 90°$; ◇, $\phi = 105°$.

5.4. *Self-excitation of circular jets*

Earlier studies of plane, circular or elliptic jets were performed with external excitation (typically by a loudspeaker) applied directly to the flow or induced by driving a settling chamber resonance. However, in technological devices, including jet aircraft, prospects for utilization of external excitation seem impractical, and one is forced to look for methods of self-excitation. We have studied self-excited air jets with whistler nozzles through flow visualization and hot-wire measurements (Hasan & Hussain 1982). From our detailed data we conclude that the whistler nozzle phenomenon is a coupling of shear-layer tone produced between the lips of the pipe nozzle and the collar, and organ-pipe resonance of the pipe nozzle. This coupling is accentuated further when the coupling frequency coincides with the preferred mode of the issuing jet. Results for a whistler nozzle are shown in figure 20 as a representative sample; the self-excitation corresponds to the preferred mode of the jet. The self-excitation clearly produces a large increase in the decay rate of the centreline mean velocity $U_c(x)$. Figure 20 also shows the $u_t'(x)$ and $U_c(x)$ without collar, under artificial excitation by a loudspeaker placed in the upstream settling chamber. The responses of the pipe nozzle to self-excitation and to artificial excitation, as represented by $u_t'(x)$, show comparable trends. When the pipe nozzle jet is forced externally, U_c drops faster with x than when unforced (data identified by circles), but this drop is never as large as that for the case of self-excitation.

There is a prospect of combining the beneficial effects of elliptic geometry and self-excitation; we are investigating elliptic whistler jets.

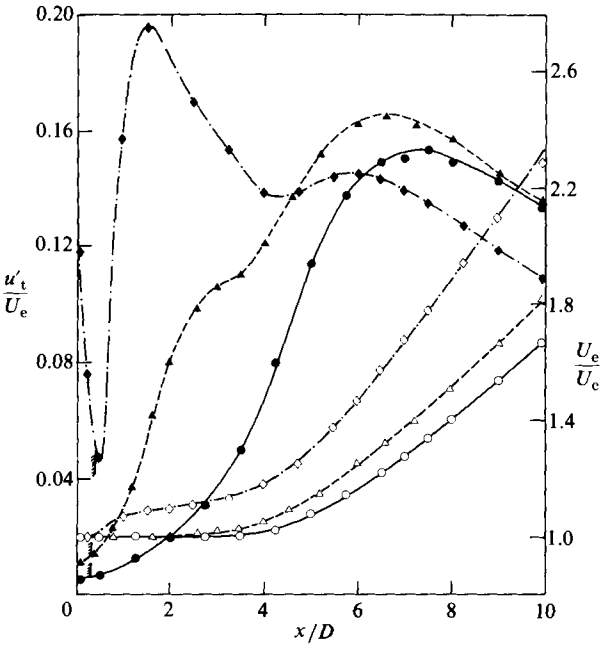

FIGURE 20. Self-excitation of a 2.54 cm circular jet showing streamwise variation of centreline mean velocity U_c (open symbols) and centreline turbulence level (solid symbols) for three different flow states. The jet exit speed $U_e = 36$ m/s; pipe nozzle length $L_p = 30.48$ cm. L_c (collar length in cm), f (frequency in Hz), and U'_c/U_e are: ○ (0.812, 0, 0.007); △ (0.83, 516, 0.011): ◇ (0.99, 504, 0.12).

6. Concluding remarks

It is the recognition of the preponderant occurrence and dominant dynamical role, rather than the discovery, of coherent structures which has injected new momentum into turbulence research and has fostered renewed hope for understanding and perhaps developing a viable theory of turbulence. The excitement and arguments over what coherent structures really are seem to have subsided somewhat – not because of apathy, but because the field has matured considerably. Now it is not worthwhile to argue when coherent structures were discovered and who should get credit, but rather, how can we better understand them and what can we do with them?

The definition of coherent structures in terms of coherent vorticity may lead to formulation of a theory perhaps based on the well-developed concepts of vortex dynamics (e.g. Hunt 1985). Unfortunately, the fact that the structures are intensely three-dimensional makes such efforts challenging, even if viscosity could indeed be ignored at these large scales. To aid in the sorely needed theoretical developments, one needs to know much more about the structures themselves. The overwhelming majority of the studies of coherent structures to date have been based on flow visualization and not on quantitative data. Motivated by convenience, flow visualization of coherent structures has been performed only at low Reynolds numbers. But caution is in order against the common temptation to interpret high-Reynolds-number flows in terms of observations made at low Reynolds numbers. Even at low Reynolds numbers, flow visualization can be highly misleading because of the high Schmidt number of the markers and history integration effect from the point of injection. Furthermore, flow visualization in fully turbulent flows is seldom enlight-

ening due to the overabundance of (typically confusing) information presented to the eye. Thus, flow visualization should be used whenever possible, but only as a supplement to quantitative data.

The crucial need is hard data, but the requirements are forbidding. Classification of all advected structures by modes and parameter sizes is necessary before a particular subclass can be focused on. Then, to capture the detailed measures of the selected structure subclass over its three-dimensional extent and to base the detection on coherent vorticity, one must in principle have a large number of vorticity probes in a three-dimensional array. The classification is simplified by invoking the existence of 'preferred modes', and the measurement challenge is eased by assuming large-scale quasi-two dimensionality and using a single transverse rake of cross-wires. Even under this restrictive assumption, spanwise contortions, induced by longitudinal ribs, are bound to occur, and one must shift structures in the spanwise direction for proper alignment before taking ensemble average. While the use of multiple rakes of sensors will facilitate acceptance of structures which can then be properly aligned with respect to each other, it seems that optical techniques like scanning two-colour LDA, particle displacement velocimetry, pulsed laser holography, or other particle tracking methods (such as nuclear magnetic resonance) hold the key to future breakthroughs in spatial measurements of time-dependent turbulent flow features, in particular coherent structures. The measurement constraints regarding resolution of sensors as well as fineness of classification force one to recognize that the coherent structure measures we obtain are inherently approximate.

Supercomputers add a new dimension to our research capability in turbulence and in coherent structures. They can complement experimental efforts in numerically computing quantities such as vorticity, pressure, enstrophy, helicity, dissipation, etc., which are extremely difficult, if not impossible, to measure in the laboratory. The current computing power is indeed limiting both in resolution (hence flow Reynolds number) and in record length, yet the results are extremely encouraging. I expect to see a lot more collaboration between experimentalists and numerical analysts, and combined efforts involving direct numerical simulation and multi-sensor measurements. In this connection, turbulent flow topology is an emerging field of inquiry, and one of the critical properties to be computed is helicity. The spatial separation of dissipation and helicity peaks, though qualitatively demonstrated, is still an open question and needs to be established conclusively for fully developed turbulent shear flows.

The question naturally arises: What should one do with all the details of coherent structures? One can easily get buried in exploring and documenting the 'anatomical details' of structures, while losing track of the objective with which one started the research or never finding any use for the data.

Coherent structures, presumably being the tractable part of turbulence, may contain most of the essential physics of turbulence. Thus, understanding the dynamics of coherent structures is adequate motivation in itself. How the 'anatomical details' will be incorporated into a viable theory is not clear, but such a theory must be cognizant of the topography and dynamical roles of coherent structures, because a turbulence theory formulated without these details will be devoid of the physics and cannot be expected to be generic, robust, helpful or even useful.

The coherent-structure approach to turbulent shear flows should not be viewed as merely of conceptual or academic interest; this approach is of profound practical significance for the understanding, design and safety of natural and man-made systems involving turbulent flows. The understanding of coherent structures clearly

holds the key to understanding turbulence management and control. Manipulation and control of turbulence has already shown evidence of payoffs and holds out hope for greater successes in a variety of technological situations involving heat, mass and momentum transport, in particular drag, combustion and aerodynamic noise. We expect to see in the near future significant thrusts and accomplishments in turbulence management via coherent structure manipulation using active and passive controls. Even without these technological benefits the study of coherent structures in turbulent shear flows is highly interesting and deserves to be pursued vigorously. Turbulence may indeed continue to remain nature's best-kept secret, but we should persist in our efforts to unveil these secrets. Studies of coherent structures very much represent the spirit and style of G. I. Taylor.

General papers like this one are bound to reflect the accumulation of many years of experience in the laboratory and results of discussions, sometimes debates, with many colleagues, both from one's own laboratory and outside. Such has been my experience. I cannot do justice in acknowledging all the fellow researchers, but feel specially indebted to: Drs R. W. Metcalfe, K. B. M. Q. Zaman, S. J. Kleis, L. S. G. Kovasznay, J. Tso, M. Hayakawa, R. Takaki and T. B. Benjamin, for many fruitful discussions. Many researchers and peers have helped in sharpening some of our ideas through comments at different times; to mention a few: Drs R. Narasimha, S. Corrsin, J. F. Foss, F. K. Browand, I. Wygnanski, A. Michalke, J. Kim and D. Coles. This manuscript has been reviewed by Dr H. S. Husain and by Messrs J. E. Bridges, J. P. Jenkinson and J. G. Broze, who have provided many helpful suggestions. No less is my gratitude to my other fellow researchers (identifiable from cited references) and students, who are my true teachers. Research reviewed here has been supported at different times by ONR, NSF and NASA. Preparation of this manuscript has been supported by Dr M. M. Reischman through the ONR Grant N00014-85-K-0126 and by Dr Ed Rice through the NASA Grant NAG3-408.

Appendix A. Flow field decompositions

Triple decomposition. In this formalism, a turbulent shear flow is decomposed into time-mean and time-dependent flows, the latter being in turn a superposition of coherent perturbation and incoherent turbulence. That is, an instantaneous flow variable f is decomposed as

$$f(\boldsymbol{x},t) = \bar{f}(\boldsymbol{x}) + f_{\mathrm{c}}(\boldsymbol{x},t) + f_{\mathrm{r}}(\boldsymbol{x},t), \tag{A1}$$

where $\bar{f}$, f_{c} and f_{r} are time-mean, coherent and incoherent turbulence components. Thus,

$$\langle f \rangle = f + f_{\mathrm{c}}, \quad f_{\mathrm{r}} = f - \langle f \rangle, \tag{A2}$$

$\langle\ \rangle$ means phase average, i.e. ensemble average of all (successive) structures at the same age or phase in their evolution. The triple decomposition is similar to that used by Reynolds & Hussain (1972) to study the mechanics of waves in turbulent shear flows.

Double decomposition. In this view, a turbulent shear flow is treated as a superposition of coherent structures and incoherent turbulence, i.e.

$$f(\boldsymbol{x},t) = \langle f \rangle(\boldsymbol{x},t) + f_{\mathrm{r}}(\boldsymbol{x},t). \tag{A3}$$

The evolutions of coherent structures and incoherent turbulence and their interactions can be explored by deriving the continuity, momentum, energy, vorticity and

enstrophy equations for the three fields in triple decomposition and the two fields in double decomposition; some of these have been discussed by Hussain (1983*a*).

The double decomposition does not acknowledge the presence of a 'time-mean' flow and thus is more realistic; however, it does not address the growth of coherent motion. The triple decomposition, on the other hand, can provide an explanation for the growth of coherent structures by the extraction of kinetic energy from the time-mean field. However, such an interpretation is meaningful only when the coherent structures are small perturbations of the mean flow. In many cases the coherent structures are highly dominant. That is, in many cases they are not perturbations of the time-mean flow: they are the flow.

Appendix B. Coherent vorticity dynamics and incoherent turbulence

Under the triple decomposition of instantaneous velocities and vorticities

$$u_i(\boldsymbol{x},t) = U_i(\boldsymbol{x}) + u_{ci}(\boldsymbol{x},t) + u_{ri}(\boldsymbol{x},t); \quad \omega_i(\boldsymbol{x},t) = \Omega_i(\boldsymbol{x}) + \omega_{ci}(\boldsymbol{x},t) + \omega_{ri}(\boldsymbol{x},t), \tag{B1}$$

The governing equation for coherent vorticity perturbation is

$$\begin{aligned}\frac{D\omega_{ci}}{Dt} = {} & \omega_{cj}\frac{\partial U_i}{\partial x_j} + \Omega_j\frac{\partial u_{ci}}{\partial x_j} + \nu\frac{\partial^2}{\partial x_j\,\partial x_j}\omega_{ci} + \frac{\partial}{\partial x_j}(u_{ci}\,\omega_{cj} - \overline{u_{ci}\,\omega_{cj}}) \\ & - \frac{\partial}{\partial x_j}(\omega_{ci}\,u_{cj} - \overline{\omega_{ci}\,u_{cj}}) - \frac{\partial}{\partial x_j}(u_{cj}\,\Omega_i) \\ & + \frac{\partial}{\partial x_j}(\langle u_{ri}\,\omega_{rj}\rangle - \overline{u_{ri}\,\omega_{rj}}) - \frac{\partial}{\partial x_j}(\langle \omega_{ri}\,u_{rj}\rangle - \overline{\omega_{ri}\,u_{rj}}),\end{aligned} \tag{B2}$$

where $\mathrm{D}/\mathrm{D}t = \partial/\partial t + U_j\,\partial/\partial x_j$. Note that summation is not implied by subscripts c and r. The significance of each term is fairly obvious. The left-hand side represents the change of coherent vorticity in a frame advected with the time-mean velocity $U(\mathbf{x})$. The successive terms on the right-hand side are: augmentation of coherent vorticity by stretching by time-mean flow, creation of coherent vorticity by stretching of mean vorticity by coherent velocity, viscous diffusion of coherent vorticity, coherent vorticity augmentation by stretching by coherent motion, advection of coherent vorticity by coherent motion, advection of mean vorticity by coherent motion, and organization by the coherent structure of: incoherent vortex stretching by incoherent turbulence and transport of incoherent vorticity by incoherent turbulence. The discussion can be further particularized and the equation simplified for specific flows. For convenience, we will discuss simplifications following the double-decomposition approach only.

The double decomposition is perhaps more appropriate for our physical perception of coherent vorticity dynamics. Thus with

$$u(\boldsymbol{x},t) = \langle u\rangle(\boldsymbol{x},t) + u_{\mathrm{r}}(\boldsymbol{x},t); \quad \omega(\boldsymbol{x},t) = \langle\omega\rangle(\boldsymbol{x},t) + \omega_{\mathrm{r}}(\boldsymbol{x},t), \tag{B3}$$

the equation for coherent vorticity becomes

$$\frac{\hat{\mathrm{D}}}{\mathrm{D}t}\langle\boldsymbol{\omega}\rangle = \langle\boldsymbol{\omega}\rangle\cdot\nabla\langle\boldsymbol{u}\rangle + \nu\nabla^2\langle\boldsymbol{\omega}\rangle + \langle\boldsymbol{\omega}_{\mathrm{r}}\cdot\nabla\boldsymbol{u}_{\mathrm{r}}\rangle - \langle\boldsymbol{u}_{\mathrm{r}}\cdot\nabla\boldsymbol{\omega}_{\mathrm{r}}\rangle. \tag{B4}$$

Here $\hat{\mathrm{D}}/\mathrm{D}t = \partial/\partial t + \langle u_j\rangle\,\partial/\partial x_j$ denotes the material derivative following the coherent flow field. It is clear that coherent vortex stretching, i.e. augmentation of coherent vorticity by its stretching by coherent motion, is not the only mechanism for change

of coherent vorticity. In fact, we will see that this is not even the dominant mechanism. The random stretching of random vorticity fluctuations by random velocity fluctuations and the random advection of random vorticity by random velocity fluctuations can be organized by the coherent structures in such a way as to affect the coherent vorticity field itself.

Simple reasoning can be applied to simplify (B4). If l is the characteristic size of the coherent structure and V_c is the characteristic velocity (say of the order of the mean velocity variation across a shear flow), then

$$|\langle\boldsymbol{\omega}\rangle| = O\left(\frac{V_c}{l}\right), \quad |\boldsymbol{\nabla}\langle\boldsymbol{u}\rangle| = O\left(\frac{V_c}{l}\right),$$

$$|\boldsymbol{\omega}\cdot\boldsymbol{\nabla}\langle\boldsymbol{u}\rangle| = \frac{C_1 V_c^2}{l^2}, \quad |\nu\nabla^2\langle\boldsymbol{\omega}\rangle| = O\left(\frac{\nu V_c}{l^2}\right). \tag{B5}$$

The ratio of the vortex stretching to the viscous diffusion terms is of the order of the Reynolds number of the coherent structure ($V_c l/\nu$), which is very large, i.e. coherent structure dynamics is inviscid, as is expected. Viewed another way, the ratio of structure turnover time ($\tau_c \approx l/V_c$), which is comparable to structure advection time, to the coherent vorticity diffusion time $\tau_d \approx l^2/\nu$, i.e. $\tau_c/\tau_d \approx \nu/(V_c l)$, is large. Thus viscous diffusion is too slow to affect structure dynamics.

Now, regarding random vorticity and velocity we can expect

$$|\boldsymbol{\omega}_r| = O(v/\lambda) \quad \text{and } |\boldsymbol{\nabla}\boldsymbol{u}_r| = O(v/\lambda), \tag{B6}$$

where v is a measure of incoherent velocity, and λ is the Taylor microscale, i.e.

$$\overline{\left(\frac{\partial u_{ri}}{\partial x_j}\right)\left(\frac{\partial u_{ri}}{\partial x_j}\right)} \approx \frac{v^2}{\lambda^2}, \tag{B7}$$

so that $\lambda \ll l$ and $v \approx V_c$. We can now write

$$|\langle\boldsymbol{u}_r\cdot\boldsymbol{\nabla}\boldsymbol{\omega}_r\rangle| = \frac{C_2 v^2}{\lambda^2}; \quad |\langle\boldsymbol{\omega}_r\cdot\boldsymbol{\nabla}\boldsymbol{u}_r\rangle| = \frac{C_3 v^2}{\lambda^2}. \tag{B8}$$

Clearly, C_1, C_2 and C_3 are likely to be comparable and of the order of unity. (C_1 can be small; it is zero in the case of vortex rings or spanwise rolls.) It therefore follows that

$$\frac{\hat{\mathrm{D}}}{\mathrm{D}t}\langle\boldsymbol{\omega}\rangle = \langle\boldsymbol{\omega}_r\cdot\boldsymbol{\nabla}\boldsymbol{u}_r\rangle - \langle\boldsymbol{u}_r\cdot\boldsymbol{\nabla}\boldsymbol{\omega}_r\rangle. \tag{B9}$$

Thus the rate of change of coherent vorticity is a balance of two contributions of the incoherent field – the contributions brought about by organization of the incoherent field by the coherent structure itself. These two terms have interesting and rather different physical interpretations. These interpretations can be easily appreciated in a turbulent flow where the coherent structures are two-dimensional. (Even simpler is the interpretation when turbulence is considered as a perturbation of a two-dimensional time-mean flow; see Tennekes & Lumley 1974.) If the left-hand side can be viewed as a spatial derivative of coherent momentum, the right-hand side can be related to the gradient of incoherent Reynolds stress organized by coherent structures. To show this, since the only component of coherent vorticity $\langle\omega\rangle_3 = \Omega$ is of interest in the case of plane shear, we have

$$\frac{\hat{\mathrm{D}}\Omega}{\mathrm{D}t} = \frac{\partial}{\partial x_j}(\langle\omega_{rj}\, u_{3r}\rangle - \langle u_{rj}\,\omega_{3r}\rangle). \tag{B10}$$

If we neglect gradients of dynamic pressure, (B 10) becomes

$$\frac{\hat{\mathrm{D}}\Omega}{\mathrm{D}t} = \left(\frac{\partial^2}{\partial x^2} - \frac{\partial^2}{\partial y^2}\right)\langle -u_r v_r \rangle. \tag{B 11}$$

Going back to (B 9), $\langle \boldsymbol{\omega}_r \cdot \nabla \boldsymbol{u}_r \rangle$ can be viewed as contributing to the loss of coherent vorticity by the organization of *stretching* of incoherent vorticity by incoherent turbulence. On the other hand, $\langle \boldsymbol{u}_r \cdot \nabla \boldsymbol{\omega}_r \rangle$ is the organization by coherent structure of the transport of incoherent vorticity by incoherent turbulence; this transport is by the vortex forces $\boldsymbol{u} \wedge \boldsymbol{\omega}$ which is analogous to (the half of) the Coriolis force on a fluid particle moving with velocity $\boldsymbol{u}$ in a frame rotating with angular velocity $\boldsymbol{\omega}$. That is, $\langle \boldsymbol{u}_r \cdot \nabla \boldsymbol{\omega}_r \rangle$ represents the essence of the vorticity transport theory of Taylor (1935); it is clear that the vorticity transport theory ignored the crucial mechanism of vortex stretching!

REFERENCES

Anderson, A. B. C. 1954 *J. Acoust. Soc. Am.* **26**, 21.

Antonia, R. A. 1981 *Ann. Rev. Fluid Mech.* **13**, 131.

Antonia, R. A., Satyaprakash, B. & Hussain, A. K. M. F. 1982 *J. Fluid Mech.* **119**, 55.

Batchelor, G. K. 1967 *An Introduction to Fluid Dynamics*. Cambridge University Press.

Batchelor, G. K. & Proudman, I. 1954 *Q. J. Mech. Appl. Maths* **7**, 83.

Beguier, C., Giralt, F., Fulachier, L. & Keffer, J. F. 1977 *Lecture Notes in Physics*, vol. 76, p. 22. Springer.

Bernal, L. P. & Roshko, A. 1986 *J. Fluid Mech.* **170**, 499.

Bradshaw, P. 1966 *J. Fluid Mech.* **26**, 225.

Bradshaw, P., Ferriss, D. H. & Johnson, R. F. 1964 *J. Fluid Mech.* **19**, 591.

Brandstäter, A., Swift, J., Swinney, H. L. & Wolf, A. 1983 *Turbulence and Chaotic Phenomena in Fluids* (ed. T. Tatsumi), p. 179. North-Holland.

Bridges, J. E. & Hussain, A. K. M. F. 1986 *J. Sound Vib.* (to appear).

Browand, F. K. & Laufer, J. 1975 *Turbulent Liquids*, p. 333. University of Missouri-Rolla.

Browand, F. K. & Troutt 1985 *J. Fluid Mech.* **158**, 489.

Browand, F. K. & Weidman, P. D. 1976 *J. Fluid Mech.* **76**, 127.

Brown, G. B. 1935 *Phys. Soc.* **47**, 703.

Brown, G. L. & Roshko, A. 1974 *J. Fluid Mech.* **64**, 775.

Cantwell, B. 1981 *Ann. Rev. Fluid Mech.* **13**, 457.

Cantwell, B. & Coles, D. 1983 *J. Fluid Mech.* **136**, 321.

Cantwell, B., Coles, D. & Dimotakis, P. E. 1978 *J. Fluid Mech.* **87**, 641.

Cimbala, J. M. 1984 Ph.D. thesis, California Institute of Technology.

Champagne, F. H. 1978 *J. Fluid Mech.* **86**, 67.

Clark, A. R. 1979 Ph.D. thesis, University of Houston.

Coles, D. 1981 *Proc. Ind. Acad. Sci.* **4**, 111.

Coles, D. 1983 *Turbulence and Chaotic Phenomena in Fluids* (ed. T. Tatsumi), p. 397. North-Holland.

Coles, D. 1985 Dryden Lecture, A.I.A.A.

Crighton, D. G. 1981 *J. Fluid Mech.* **106**, 261.

Crow, S. C. 1970 *AIAA J.* **8**, 2172.

Crow, S. C. & Champagne, F. H. 1971 *J. Fluid Mech.* **48**, 547.

Davis, S. H. 1976 *Ann. Rev. Fluid Mech.* **8**, 57.

Dimotakis, P. E., Miake-Lye, R. C. & Papantoniou, D. A. 1983 *Phys. Fluids* **26**, 3185.

Dimotakis, P. E., Lye, R. C. & Papantoniou, D. A. 1982 *An Album of Fluid Motion* (ed. M. Van Dyke), p. 97. Parabolic.

FIEDLER, H. E., DZIOMBA, B., MENSING, P. & ROSGEN, T. 1980 *Lecture Notes in Physics*, vol. 136, p. 219. Springer.

FISHER, M. J. & DAVIES, P. O. A. L. 1964 *J. Fluid Mech.* **18**, 97.

FFOWCS-WILLIAMS, J. E. & KEMPTON, A. J. 1978 *J. Fluid Mech.* **84**, 673.

FOSS, J. F. 1977 *Turbulent Shear Flows*, p. 11.33. Pennsylvania State University.

FREYMUTH, P. 1966 *J. Fluid Mech.* **25**, 683.

FRISH, M. B. & WEBB, W. W. 1981 *J. Fluid Mech.* **107**, 173.

GOLDSTEIN, M. E. 1984 *Ann. Rev. Fluid Mech.* **16**, 263.

GOLLUB, J. P. & BENSON, S. V. 1980 *J. Fluid Mech.* **100**, 449.

GOTTLIEB, D. & ORSZAG, S. A. 1977 *Numerical Analysis of Spectral Methods: Theory and Applications*. S.I.A.M.

GRINSTEIN, F. F., ORAN, E. S. & BORIS, J. P. 1986*a* *J. Fluid Mech.* **165**, 201.

GRINSTEIN, F. F., ORAN, E. S. & BORIS, J. P. 1986*b* *AIAA J.* (to appear).

HAMA, F. R. 1960 *Ht. Tr. & Fl. Mech. Institute*, p. 92. Stanford University.

HANJALIC, K. & LAUNDER, B. E. 1972 *J. Fluid Mech.* **51**, 301.

HAYAKAWA, M. & HUSSAIN, A. K. M. F. 1985 *Turbulent Shear Flows V*, p. 4.33. Cornell University.

HASAN, M. A. Z. 1983 Ph.D. thesis, University of Houston.

HASAN, M. A. Z. & HUSSAIN, A. K. M. F. 1982 *J. Fluid Mech.* **115**, 59.

HERNAN, M. A. & JIMENEZ, J. 1982 *J. Fluid Mech.* **119**, 323.

HESKESTAD, G. 1965 *J. Appl. Mech.* **87**, 735.

HINZE, J. O. 1975 *Turbulence*. McGraw-Hill.

HO, C. M. & HUERRE, P. 1984 *Ann. Rev. Fluid Mech.* **16**, 365.

HOWE, M. S. 1975 *J. Fluid Mech.* **85**, 685.

HUNT, J. C. R. 1973 *J. Fluid Mech.* **61**, 625.

HUNT, J. C. R. 1985 Invited Lecture at CANCAM 1985.

HUSAIN, H. S. 1984 Ph.D. thesis, University of Houston.

HUSSAIN, A. K. M. F. 1980 Lecture notes in Physics, vol. 136, p. 252. Springer.

HUSSAIN, A. K. M. F. 1981 *Proc. Ind. Acad. Sci.* **4**, 129.

HUSSAIN, A. K. M. F. 1983*a* *Phys. Fluids* **26**, 2816.

HUSSAIN, A. K. M. F. 1983*b* *Turbulence and Chaotic Phenomena in Fluids* (ed. T. Tatsumi), p. 453. North-Holland.

HUSSAIN, A. K. M. F. & CLARK, A. R. 1981 *J. Fluid Mech.* **104**, 263.

HUSSAIN, A. K. M. F. & ZAMAN, K. B. M. Q. 1980 *J. Fluid Mech.* **101**, 493.

HUSSAIN, A. K. M. F. & ZAMAN, K. B. M. Q. 1981 *J. Fluid Mech.* **110**, 39.

HUSSAIN, A. K. M. F. & ZAMAN, K. B. M. Q. 1985 *J. Fluid Mech.* **159**, 85.

JIMENEZ, J., COGOLLOS, M. & BERNAL, L. P. 1985 *J. Fluid Mech.* **152**, 125.

JUVÉ, D., SUNYACH, M. & COMTE-BELLOT, G. 1980 *J. Sound Vib.* **71**, 319.

KAMBE, T. & TAKAO, T. 1971 *J. Phys. Soc. Japan* **31**, 591.

KEFFER, J. F. 1982 In *Complex Turbulent Shear Flows*. Springer.

KERR, R. M. & GIBSON, C. H. 1985 *Bull. Am. Phys. Soc.* **30**, 1733.

KIBENS, V. 1980 *AIAA J.* **18**, 434.

KLINE, S. J., REYNOLDS, W. D., SCHRAUB, F. A. & RUNSTADLER, P. W. 1967 *J. Fluid Mech.* **30**, 741.

KO, N. W. M. & DAVIES, P. O. A. L. 1971 *J. Fluid Mech.* **50**, 49.

KOVASZNAY, L. S. G. 1977 *Symp. Turbulence*, p. 1.

LAU, J. C. 1979 *Proc. R. Soc. Lond.* A **367**, 193.

LAU, J. C. & FISHER, M. J. 1975 *J. Fluid Mech.* **67**, 229.

LAUFER, J. 1974 *Omaggio Carto Ferrari*, p. 451.

LAUFER, J. 1983 *J. Appl. Mech.* **50**, 1079.

LEVICH, E., LEVICH, B. & TSINOBER, A. 1983 *Turbulence and Chaotic Phenomena in Fluids* (ed. T. Tatsumi), p. 309. North-Holland.

LIEPMANN, H. W. 1979 *Am. Sci.* **67**, 221.

LIGHTHILL, M. J. 1952 *Proc. R. Soc. Lond.* A**211**, 564.

LIN, C. C. 1953 *Q. Appl. Maths* **18**, 295.

LIN, S. J. & CORCOS, G. M. 1984 *J. Fluid Mech.* **141**, 139.

LUMLEY, J. L. 1965 *Phys. Fluids* **8**, 1056.

LUMLEY, J. L. 1981 *Transition and Turbulence* (ed. R. E. Meyer), p. 215. Academic.

LUSH, P. A. 1971 *J. Fluid Mech.* **46**, 477.

METCALFE, R. W., HUSSAIN, A. K. M. F., MENON, S. & HAYAKAWA, M. 1986*a* *Turbulent Shear Flow*. Springer (to appear.)

METCALFE, R. W., ORSZAG, S. A., BRACHET, M. E., MENON, S. & RILEY, J. J. 1986*b* *J. Fluid Mech.* (to appear).

MICHALKE, A. 1965 *J. Fluid Mech.* **23**, 521.

MOFFATT, H. K. 1969 *J. Fluid Mech.* **35**, 117.

MOFFATT, H. K. 1983 *Turbulence and Chaotic Phenomena in Fluids* (ed. T. Tatsumi), p. 223. North-Holland.

MOFFATT, H. K. 1985 *J. Fluid Mech.* **159**, 359.

MOHRING, M. 1978 *J. Fluid Mech.* **85**, 685.

MOIN, P. & KIM, J. 1985 *J. Fluid Mech.* **155**, 441.

MOLLO-CHRISTENSEN, E. 1967 *J. Appl. Mech.* **89**, 1.

MOORE, D. W. & SAFFMAN, P. G. 1975 *J. Fluid Mech.* **69**, 465.

MUMFORD, J. C. 1982 *J. Fluid Mech.* **118**, 241.

MUMFORD, J. C. 1983 *J. Fluid Mech.* **137**, 447.

NALLASAMY, M. & HUSSAIN, A. K. M. F. 1984 *Turbulent Shear Flows*, vol. 4, p. 169. Springer.

OSHIMA, T. & ASAKA, S. 1977 *J. Phys. Soc. Japan* **42**, 708.

OBERMEIER, F. 1985 *J. Sound Vib.* **99**, 111.

PELZ, R. B., YAKHOT, V., ORSZAG, S. A., SHTILMAN, L. & LEVICH, E. 1985 *Phys. Rev. Lett.* **54**, 2505.

PELZ, R. B., SHTILMAN, L. & TSINOBER, A. 1986 *Phys. Fluids* (in press).

PERRY, A. E. & CHONG, M. S. 1982 *J. Fluid Mech.* **119**, 173.

PERRY, A. E. & TAN, D. K. M. 1984 *J. Fluid Mech.* **141**, 197.

POWELL, A. 1964 *J. Acoust. Soc. Am.* **36**, 177.

REYNOLDS, W. C. & BOUCHARD 1981 *Unsteady Turbulent Shear Flows*, p. 402. Springer.

REYNOLDS, W. C. & HUSSAIN, A. K. M. F. 1972 *J. Fluid Mech.* **54**, 263.

RIBNER, H. 1962 AFOSR TN 3430.

RILEY, J. J. & METCALFE, R. W. 1980 *AIAA paper* 80-0274.

ROCKWELL, D. & SCHACHENMANN, A. 1982 *J. Fluid Mech.* **117**, 425.

ROGALLO, R. S. & MOIN, P. 1984 *Ann. Rev. Fluid Mech.* **16**, 99.

ROSHKO, A. 1976 *AIAA J.* **14**, 1349.

SAFFMAN, P. G. 1978 *J. Fluid Mech.* **84**, 625.

SAFFMAN, P. G. 1980 *Lecture Notes in Physics*, vol. 136, p. 1. Springer.

SAFFMAN, P. G. & BAKER, G. R. 1979 *Ann. Rev. Fluid Mech.* **11**, 95.

SANO, M. & SAWADA, Y. 1983 *Turbulence and Chaotic Phenomena in Fluids* (ed. T. Tatsumi), p. 167. North-Holland.

SMITH, C. R. & ABBOTT, D. 1978 *Coherent Structures of Turbulent Boundary Layers*. Lehigh University.

SOKOLOV, M., HUSSAIN, A. K. M. F., KLEIS, S. J. & HUSAIN, Z. D. 1980 *J. Fluid Mech.* **98**, 65.

TAKAKI, R. & HUSSAIN, A. K. M. F. 1984 *Phys. Fluids* **27**, 761.

TAKAKI, R. & HUSSAIN, A. K. M. F. 1985 *Turbulent Shear Flows*, vol. 5, p. 3.19. Cornell University.

TAM, C. K. W. & MORRIS, P. J. 1985 *J. Sound Vib.* **102**, 119.

TANEDA, S. 1959 *J. Phys. Soc. Japan* **14**, 843.

TAYLOR, G. I. 1935 *Proc. R. Soc. Lond.* A**135**, 685.

TENNEKES, H. & LUMLEY, J. L. 1974 *A First Course in Turbulence.* MIT Press.

TOWNSEND, A. A. 1979 *J. Fluid Mech.* **95**, 515.

TSINOBER, A. & LEVICH, E. 1983 *Phys. Lett.* **99**A, 321.

TSO, J. 1983 PhD thesis, the Johns Hopkins University.

WALLACE, J. M. 1986 *Expt. Fluids* **4**, 61.

WIDNALL, S. E., BLISS, D. B. & TSAI, C.6Y. 1974 *J. Fluid Mech.* **66**, 35.

WINANT, C. D. & BROWAND, F. K. 1974 *J. Fluid Mech.* **63**, 237.

WYGNANSKI, I. 1985 Lecture at APS/DFD Annual Meeting, University of Arizona.

WYGNANSKI, I. & FIEDLER, H. E. 1969 *J. Fluid Mech.* **38**, 577.

WYGNANSKI, I., OSTER, D. & FIEDLER, H. 1979 *Turbulent Shear Flows II.* Imperial College.

ZAMAN, K. B. M. Q. 1985 *J. Fluid Mech.* **152**, 83.

ZAMAN, K. B. M. Q. & HUSSAIN, A. K. M. F. 1977 *Turbulent Shear Flow*, p. 11.23. Pennsylvania State University.

ZAMAN, K. B. M. Q. & HUSSAIN, A. K. M. F. 1980 *J. Fluid Mech.* **101**, 449.

ZAMAN, K. B. M. Q. & HUSSAIN, A. K. M. F. 1981 *J. Fluid Mech.* **103**, 133.

ZAMAN, K. B. M. Q. & HUSSAIN, A. K. M. F. 1984 *J. Fluid Mech.* **138**, 325.

ZILBERMAN, M., WYGNANSKI, I. & KAPLAN, R. E. 1977 *Phys. Fluids Suppl.* **20**, S258.